



**HAL**  
open science

# Sub-Riemannian geometry, Hamiltonian dynamics, micro-swimmers, copepod nauplii and copepod robot

Bernard Bonnard, Monique Chyba, Jérémy Rouot, Daisuke Takagi

## ► To cite this version:

Bernard Bonnard, Monique Chyba, Jérémy Rouot, Daisuke Takagi. Sub-Riemannian geometry, Hamiltonian dynamics, micro-swimmers, copepod nauplii and copepod robot. *Pacific Journal of Mathematics for Industry*, 2018, 10 (2), 10.1186/s40736-018-0036-9 . hal-01653901v3

**HAL Id: hal-01653901**

**<https://hal.science/hal-01653901v3>**

Submitted on 4 May 2018

**HAL** is a multi-disciplinary open access archive for the deposit and dissemination of scientific research documents, whether they are published or not. The documents may come from teaching and research institutions in France or abroad, or from public or private research centers.

L'archive ouverte pluridisciplinaire **HAL**, est destinée au dépôt et à la diffusion de documents scientifiques de niveau recherche, publiés ou non, émanant des établissements d'enseignement et de recherche français ou étrangers, des laboratoires publics ou privés.

## SURVEY

# Sub-Riemannian geometry, Hamiltonian dynamics, Micro-swimmers, Copepod nauplii and Copepod robot

Bernard Bonnard<sup>1,2</sup>, Monique Chyba<sup>4\*</sup>, Jérémy Rouot<sup>3</sup> and Daisuke Takagi<sup>4</sup>

## Abstract

The objective of this article is to present the seminal concepts and techniques of Sub-Riemannian geometry and Hamiltonian dynamics, complemented by adapted software to analyze the dynamics of the copepod micro-swimmer, where the model of swimming is the slender body approximation for Stokes flows in fluid dynamics. In this context, the copepod model is a simplification of the 3-link Purcell swimmer and is relevant to analyze more complex micro-swimmers. The mathematical model is validated by observations performed by Takagi's team of Hawaii laboratory, showing the agreement between the predicted and observed motions. Sub-Riemannian geometry is introduced, assuming that displacements are minimizing the expanded mechanical energy of the micro-swimmer. This allows to compare different strokes and different micro-swimmers and minimizing the mechanical energy of the robot. The objective is to maximize the efficiency of a stroke (the ratio between the displacement produced by a stroke and its length). Using the Maximum Principle in the framework of Sub-Riemannian geometry, this leads to analyze family of periodic controls producing strokes to determine the most efficient one. Graded normal forms introduced in Sub-Riemannian geometry to evaluate spheres with small radius is the technique used to evaluate the efficiency of different strokes with small amplitudes, and to determine the most efficient stroke using a numeric homotopy method versus standard direct computations based on Fourier analysis. Finally a copepod robot is presented whose aim is to validate the computations and very preliminary results are given.

**Keywords:** Geometric optimal control; Sub-Riemannian geometry; Optimality conditions; Direct and indirect numerical methods in optimal control; Micro-swimmers and efficient strokes; Closed geodesics in Riemannian geometry

\*Correspondence:  
chyba@hawaii.edu

<sup>4</sup>University of Hawaii, 2565  
McCarthy the Mall Department of  
Mathematics University of Hawaii  
, 96822, Honolulu, HI, USA  
Full list of author information is  
available at the end of the article

## 1 Introduction

Sub-Riemannian (SR) geometry in the framework of geometric optimal control was first explored in the seminal article [17]. This article also contains the main geometric ingredients developed in our article in relation with micro-swimmers : the Heisenberg-Brockett-Dido model and the evaluation of conjugate-cut loci and small SR-spheres using normal coordinates. These techniques were developed later in the context of singularity theory to obtain more precise computations of asymptotics of the conjugate and cut loci, in a series of articles dealing with the so-called contact Darboux case [19] and Martinet case [1]. A consequence of SR-geometry is that the singularities of the exponential mapping accumulate for small lengths and can be estimated. Clearly, this is the starting point to produce numerical computations for larger lengths by using continuation and numerical methods. Also, early on in the analysis of SR-geometries, complicated singularities (not in the "analytic" category) were recognized due to the existence of the so-called *abnormal geodesics*. This was a major technical problem to further developments for the computational

techniques. Note that the similar problem clearly stopped the activity in the fifties of the standard calculus of variations [10].

An application of SR-geometry was identified in [33] which describes the geodesics motions of a charged particle in a 2D-Riemannian manifold under the influence of a magnetic field. In this framework, closed geodesics calculations correspond precisely to stroke's computations for micro-swimmers. This is a generalization of the Dido problem in calculus of variations and a very technical study [2] using tools developed in [19], has provided the asymptotics of the conjugate and cut loci. A pause for those computations based on *symbolic* software was observed but a revival is now motivated with the development of a specific software (see [22]) based on numerical continuation methods in optimal control [3]. This has already many applications in the areas of aerospace or quantum control problems [47, 15]. Our study is a further step in this direction.

Micro-swimmers were popularized by the seminal presentation [38] and were analyzed very recently using optimization techniques in a series of articles [5, 4], motivated in particular by industrial applications in robotics to design micro-robots whose control is based on the swimming mechanisms of biological micro-swimmers. In particular a recent model was proposed in [41] to analyze the observed motions of an abundant variety of zooplanktons called copepods. Assuming the motion is performed to minimize the mechanical energy dissipated by the swimmer, the problem of determining the most efficient stroke can be analyzed in the framework of SR-geometry.

It can be compared with the standard methods in fluid dynamic, using direct optimization methods, and based on Fourier expansions to represent strokes [42]. Our method of analysis developed for the copepod model is entirely different and uses an indirect optimization method. The candidates as minimizers are parameterized as geodesics of the associated SR-problem using the Maximum Principle, and already a discrimination is obtained between the normal geodesics associated to smooth periodic controls and a unique abnormal geodesic whose shape corresponds to a triangle and observed in [41] as a pattern of the copepod strokes. The concept of efficiency can be reformulated in SR-geometry as the ratio between the displacement produced by a stroke and its length. A consequence of the Maximum Principle and the so-called *transversality condition* is that the most efficient stroke can be computed using a numerical shooting. It can be also determined using numerical continuation techniques starting from a center of swimming (a center of swimming being a point from which are emanating strokes with small amplitudes). The latter is computed as an invariant of SR-geometry. This study is related to the conjugate and cut loci computation [2] which are also important to analyze optimality and convergence of the numerical optimization methods. Direct optimization methods implemented in the `Bocop` software [11] were applied in [8] to initialize the continuation starting near the abnormal stroke with maximum amplitude. Note that our approach is closely related to the seminal work in celestial mechanics by Poincaré [36] combining already direct and indirect approaches in variational analysis. In particular our result is reminiscent of the Poincaré-Lyapunov theorem where periodic trajectories are obtained by continuation as a one parameter family of periodic trajectories with small amplitudes emanating from a center [32].

*Structure of the paper.* In section 2, the various swimmer's models are presented using Resistive Force Theory approximation [24],[21, Chapter 5] governing the swimmer mechanism at low Reynolds number where the interaction with the fluid is reduced to a drag force [6] and the swimmer is represented using a slender body approximation. The remaining of the section is to describe the geometric framework of the problem and the associated optimal control problem. The section 3 is a self-contained presentation of SR-geometry to describe the concepts and technical tools necessary to our study. The following concepts are borrowed from geometric optimal control: Maximum Principle, Second order necessary optimality conditions (Jacobi equation, notion of conjugate point). The remaining ones are specific to SR-geometry: nilpotent approximation, generic graded normal forms and applications to estimate the SR-spheres with small radius. Section 4 is devoted to the complete analysis of the copepod swimmer, applying the mathematical tools mentioned above supplemented with numerical simulations to compute the center of swimming for strokes with small amplitudes and to eventually determine the most efficient stroke. The final section is devoted to present the agreement between control practitioners and experiments. It is realized in two steps. First of all, to validate the model of swimming at low Reynolds number (using slender body theory for stokes flow), we present the agreement between predicted and observed displacements of the copepod nauplii (a three pair of symmetric links swimmers). Secondly to compare different stroke and different swimmers a macroscopic copepod robot is finally described to validate in a next future the agreement between control computation, simulations and experiments. Preliminary results are presented.

## 2 Micro-swimmers and the geometric framework

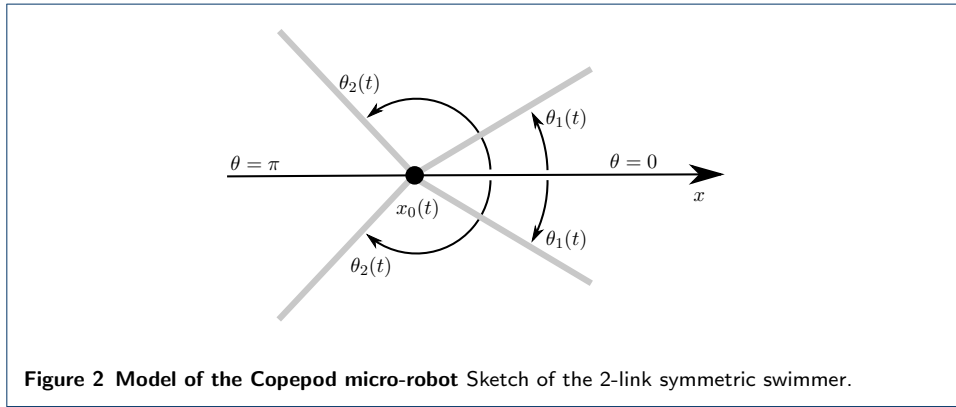
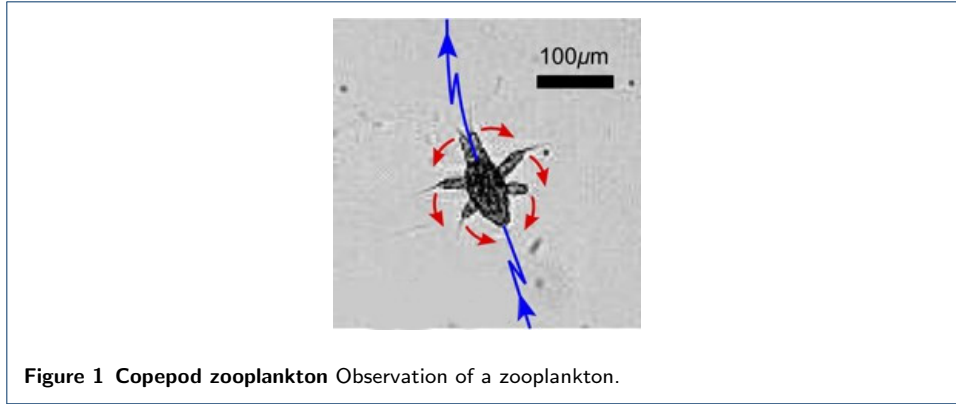
This section is a self-contained presentation of micro-swimmers related to our study and the standard geometric properties contained in the literature which allows for a neat analysis in the framework of direct optimization methods.

### 2.1 n-links swimmers

Studying micro-swimmers is motivated by biological observations as well as engineering applications to design aquatic robots swimming at low Reynolds numbers which corresponds to micro-robots or robots in viscous fluid such as glycerine. Swimming at Low Reynolds number in hydrodynamics is modelled by Stokes equations and for a self-propelled organism its movement is produced by shape deformation called a stroke, we refer to [6] for a complete description. Toward the construction of simple robots, we restrict ourselves to n-links swimmers for which the slender body approximation is valid [34]. We will focus on the copepod swimmer which has recently gained interest in the literature, see [41, 29]. The mathematical model described in [41] consists of n-pairs of symmetric (slender) legs with the body being reduced to a small sphere with radius  $r$ . The copepod zooplankton and the associated micro-robot are represented in Fig.1 and Fig.2. See Section 5.1 for a brief description of the general case.

#### 2.1.1 Stokes model

By symmetry, the displacement takes place along a line  $Ox_0$ , and assuming  $r = 0$  (negligible body size) the slender body approximation for Stokes flow reduces the



equation for the displacement variable (swimming velocity) to:

$$\dot{x}_0 = \frac{\sum_{i=1}^n \dot{\theta}_i \sin \theta_i}{\sum_{i=1}^n (1 + \sin^2 \theta_i)}. \quad (1)$$

Introducing the control formalism, the dynamics of the shape variables  $\theta = (\theta_1, \dots, \theta_n)$  is given by  $\dot{\theta}_i = u_i$ . We denote by  $q = (x_0, \theta)$  the state vector, and the equations of motion are expressed as a *driftless control system*:

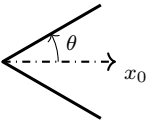
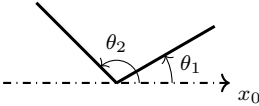
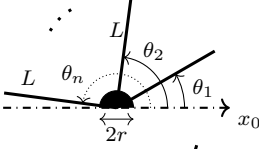
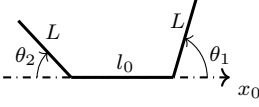
$$\dot{q} = \sum_{i=1}^n u_i F_i(q). \quad (2)$$

**Definition 1** A (smooth) stroke is a periodic motion  $t \mapsto \theta(t)$  produced by a (smooth) periodic control  $t \mapsto u(t)$ , with period  $T > 0$ .

For  $n = 1$ , the model depicts a *scallop* where each stroke produces a zero displacement. This is known in the literature as the famous *scallop theorem*.

Hence at least two legs,  $n \geq 2$ , are required to produce a positive displacement and the copepod observed in Fig. 1 corresponds to  $n = 3$  for which the swimming mechanism is described and analyzed in [29, 41].

Our objective is to make a complete analysis of the case  $n = 2$ , in the framework of SR-geometry. Note that this case was also obtained in [5] as a limit case of

<ul style="list-style-type: none"> <li>• Scallop</li> </ul>		$\dot{x}_0 = \frac{\dot{\theta} \sin \theta}{2 - \cos^2 \theta}$
<ul style="list-style-type: none"> <li>• Symmetric 2-links Copepod</li> </ul>		$\dot{x}_0 = \frac{\sum_{i=1}^2 \dot{\theta}_i \sin \theta_i}{\sum_{i=1}^2 (1 + \sin^2 \theta_i)}$
<ul style="list-style-type: none"> <li>• Symmetric Takagi <math>n</math>-links equal lengths <math>L = 1</math></li> </ul>		$\dot{x}_0 = \frac{(1 + 2r) \sum_{i=1}^n \dot{\theta}_i \sin \theta_i}{3/2 r \log(2/r) \sum_{i=1}^n (1 + \sin^2 \theta_i)}$
<ul style="list-style-type: none"> <li>• Symmetric Purcell (Avron-Raz), 2-links equal lengths <math>L = 1</math></li> </ul>		$dx_0 = \frac{d\xi_1 + d\xi_2}{4 + c - \xi_1^2 - \xi_2^2}$ $\xi_i = \cos \theta_i, c = l_0/2$

Limit case:  $c = r = 0 \Rightarrow$  Takagi = Purcell.

**Table 1** Models of symmetric swimmer encountered in the literature.

the symmetric Purcell swimmer, with equal arms-legs lengths and zero central link length. It was analyzed by direct optimization methods.

We summarize in Table 1 the various models of symmetric (slender body) swimmers encountered in the literature.

### 2.1.2 Physical limitations and state constraints

A singularity of the models occurs when two of the links are colliding. To avoid this issue, we impose the following state constraints defined by the *triangle of constraints*:  $\mathcal{T} = \{\theta, 0 \leq \theta_1 \leq \theta_2 \leq \pi\}$ . The physical interpretation is well described in the literature. It is the so-called "Cox-theory": to neglect the physical interaction between the links they must be at a minimal distance from each other [23]. From the mathematical point of view, (1) can be analytically extended to the 2-dimensional plane where  $\mathbb{R}^2$  is taken as the covering space of the  $\theta$ -space: the torus  $\mathbb{T}^2$ . Hence  $\mathcal{T}$  is considered as a state constraints and it will be shown that this constraint is not active in our study, i.e. we will demonstrate that an optimized stroke satisfies the Cox conditions by estimating the distance to the triangle.

Note also that the extension of the dynamics to  $\mathbb{R}^2$  leads to preserve symmetries with respect to the sides of the triangles generated by  $\sigma_1 : (\theta_1, \theta_2) \mapsto (\theta_2, \theta_1)$ ,  $\sigma_2 : (\theta_1, \theta_2) \mapsto (-\theta_1, \theta_2)$ . Another observed symmetry preserving the triangle constraint is given by:  $\sigma_3 : (\theta_1, \theta_2) \mapsto (\pi - \theta_2, \pi - \theta_1)$ . The group generated by such symmetries is denoted  $\Sigma$ .

### 2.1.3 Riemannian metrics in the shape variables

A natural metric introduced in the literature is the *mechanical energy* dissipated by the swimmer, see [42]. For the copepod model, it is equivalent to minimize the mechanical energy dissipated by the pairs of legs. The associated metric is given by  $g_M = \dot{q}M\dot{q}^T$  [41], where

$$M = \begin{pmatrix} 2 - \frac{1}{2}(\cos^2 \theta_1 + \cos^2 \theta_2) & -\frac{1}{2} \sin \theta_1 & -\frac{1}{2} \sin \theta_2 \\ -\frac{1}{2} \sin \theta_1 & \frac{1}{3} & 0 \\ -\frac{1}{2} \sin \theta_2 & 0 & \frac{1}{3} \end{pmatrix}. \quad (3)$$

Using (1) it can be written as:

$$g_M = a(q) u_1^2 + 2b(q) u_1 u_2 + c(q) u_2^2$$

where

$$a = \frac{1}{3} - \frac{\sin^2 \theta_1}{2 \Delta(\theta)}, \quad b = -\frac{\sin \theta_1 \sin \theta_2}{2 \Delta(\theta)},$$

$$c = \frac{1}{3} - \frac{\sin^2 \theta_2}{2 \Delta(\theta)}, \quad \Delta(\theta) = 2 + \sin^2 \theta_1 + \sin^2 \theta_2.$$

This metric can also be extended to the entire *covering space*  $\mathbb{R}^2$  with the symmetries induced by the group  $\Sigma$ . Our study can be generalized by taking into account any choice of Riemannian metric in the shape space with similar symmetries, and the geometric analysis is similar for any choice. Another metric of particular interest, helping to simplify calculations and to perform numerical computations, is the *flat* or *Euclidean metric*:

$$g_E = u_1^2 + u_2^2.$$

## 2.2 Geometric framework

Having introduced the model, some insights about the problem can be derived from the geometric framework that we present next. This is crucial to understand the problem in relation with standard similar studies, see for instance [33, 5], for more details.

### *The swimming curvature*

Assume a stroke denoted  $\gamma$  with period  $T$ . Using (1), the associated displacement produced by this stroke is given by:

$$x_0(T) - x_0(0) = \oint_{\gamma} \omega$$

where  $\omega$  is the smooth one-form

$$\omega = \sum_{i=1}^2 \frac{\sin \theta_i}{\Delta(\theta)} d\theta_i.$$

We assume the stroke  $\gamma$  to be a piecewise smooth curve and we denote by  $D$  the domain bounded by  $\gamma$ . Using Green's theorem, we have:

$$x_0(T) - x_0(0) = \oint_{\gamma} \omega = \int_D d\omega.$$

We introduce

$$f(\theta) = \frac{2 \sin \theta_1 \sin \theta_2 (\cos \theta_1 - \cos \theta_2)}{\Delta(\theta)^2}$$

and an easy calculation provides the following lemma.

**Lemma 1**

- 1  $d\omega = -f(\theta)d\theta_1 \wedge d\theta_2$
- 2  $d\omega < 0$  in the interior of the triangle  $\mathcal{T}$ , and  $d\omega$  vanishes on the boundary of  $\mathcal{T}$ .

*Geometric consequence.* Restricted to the interior of  $\mathcal{T}$ ,  $d\omega$  is a volume form (density) which allows to estimate the displacement associated to *small (amplitudes) strokes*. It can be "normalized" to have an *invariant meaning* using the 2-form associated to a general Riemannian metric:

$$g : E(\theta)u^2 + 2G(\theta)uv + F(\theta)v^2$$

defined as

$$\omega_g = \sqrt{EF - G^2} d\theta_1 \wedge d\theta_2. \quad (4)$$

This leads to introduce the following concepts.

**Definition 2**

- 1 A *geometric 2-link micro-swimmer* is defined by  $(d\omega, g)$ .
- 2 The *swimming curvature* is defined as the ratio:

$$SK = \frac{d\omega}{\omega_g} = -\frac{f(\theta)}{\sqrt{E(\theta)F(\theta) - G(\theta)^2}}.$$

- 3 The *geometric efficiency* of a stroke  $\gamma$  is the ratio between the displacement and the length  $l$ :

$$\mathcal{E}(\gamma) = (x_0(T) - x_0(0))/l(\gamma).$$

*Applications.* A standard illustration found in the literature is the representation of the level sets of  $SK$  in the shape space and to compute the extrema. It can be observed on Fig.4 with the level sets contained in the triangle  $\mathcal{T}$  respectively for the Euclidean energy and the mechanical energy case.

Extension of two form on the covering space is represented in Fig.3.

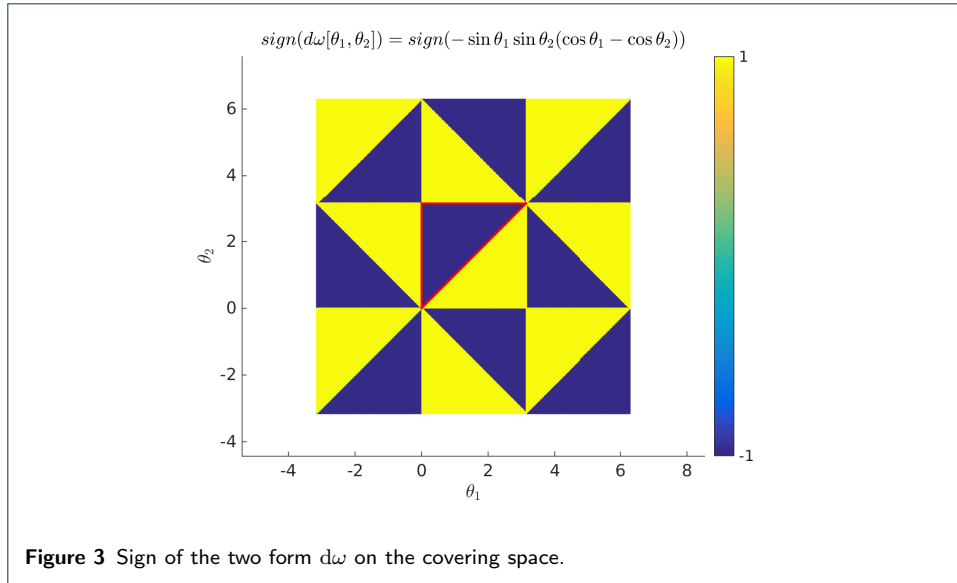
**2.2.1 Geometric optimal control problems**

*Problem 1* The first problem which can be phrased in the framework of SR-geometry is to fix the initial condition  $q(0) = (x_0(0) = 0, \theta(0))$  and compute the SR-spheres of radii  $r$  to identify the closed curves corresponding to smooth periodic controls producing a desired displacement  $x_0(T)$ . This formulation leads to the Ambrose-Singer theorem in relation with the Chow theorem in control theory, see [33].

*Problem 2* The second problem is to compute the most efficient stroke.

Both problems lead to *Mayer problems* in optimal control theory.





*Optimal Control Theory (OCT) formulation.* The extended dynamics is given by

$$\dot{q} = F(q, u), \quad (5)$$

$$\dot{q}_0 = g(u) \quad (6)$$

with  $q_0(0) = 0$ . The cost to minimize is of the form

$$C(q(T), q_0(T))$$

with prescribed boundary conditions  $x_0(0) = 0, \theta(0) = \theta(T)$ .

*Problem 1* The cost is taken as  $C = q_0(T)$  and we have  $x_0(T) = x_T$  where  $x_T$  is given.

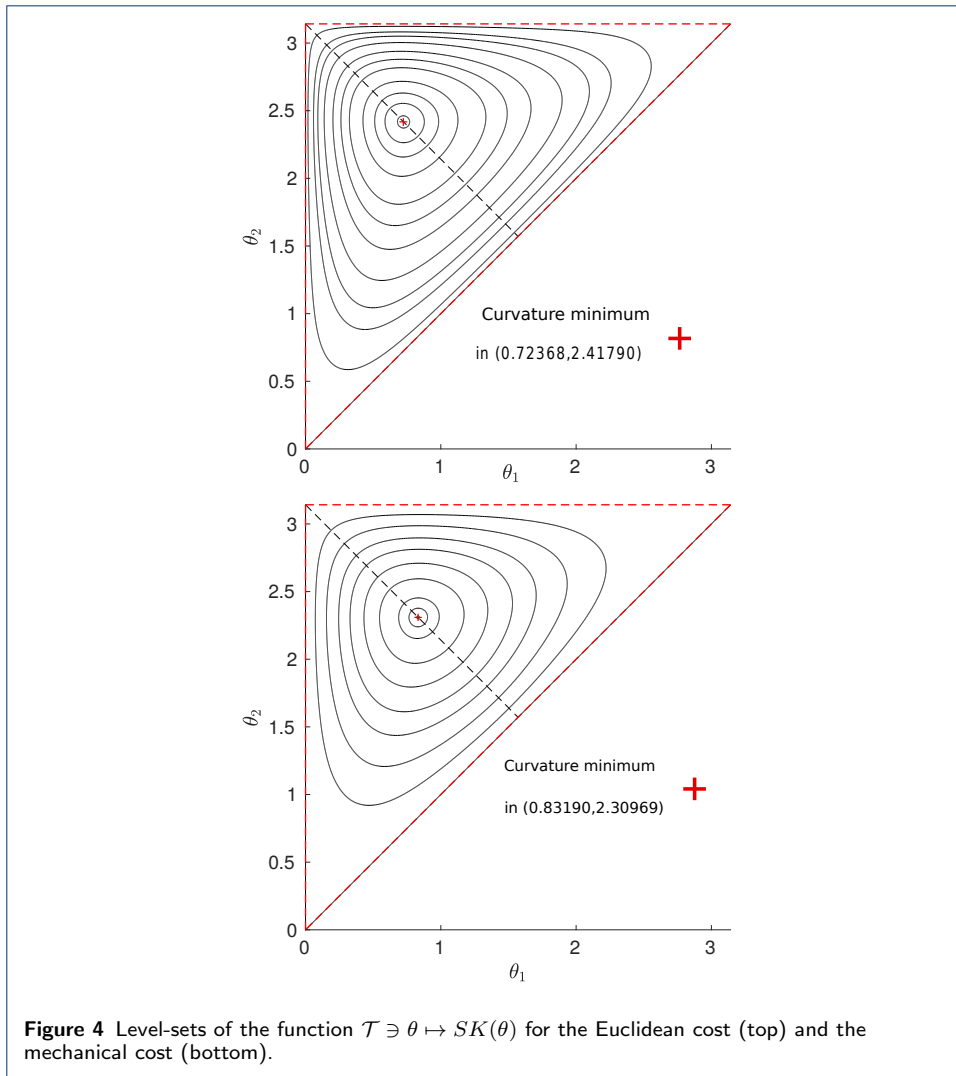
*Problem 2* The cost is taken as  $C = -x_0(T)/q_0(T)$ .

**Remark 1** In the standard literature [30, 42] the efficiency is the ratio between the square of the displacement and the energy (vs length). Parameterizing by arc-length leads to proportional quantities and similar minimizers. It allows for different kind of strokes for one species (e.g. copepod) or different species to determine the time minimizer (winning the competition).

*Program.* The work is clear, we must conduct a careful analysis in the framework of SR-geometry based on the mathematical analysis of the geodesics equation. It needs to be supplemented by (simple) numerical simulations for solving problems 1 and 2.

### 3 A review of SR-geometry in relation with micro-swimmers

SR-geometry is a very active area of research and we refer the reader to [25] for a recent and more complete presentation. Our task is limited to a specific problem



and we shall restrict our presentation to the useful concepts and results of this large area. The main concepts and seminal results were already available at the end of the nineties and general and useful references are [7, 27]. Other tools are borrowed from singularity theory, we refer the reader to [31] for a general reference and to [45] for the application to Legendrian and Lagrangian singularities.

### 3.1 General results and concepts in SR-geometry

Even locally, SR-geometry is a very rich and intricate geometry (with many invariants). It is defined by a smooth triplet  $(U, D, g)$  where  $U$  is an open subset in  $\mathbb{R}^n$ ,  $D$  is a constant rank  $m$ -dimensional distribution defined by  $\text{span}\{F_1(q), \dots, F_m(q)\}$  where  $F_i$ 's are (smooth) vector fields on  $U$  and  $g$  is the restriction of a (smooth) Riemannian metric on  $U$  to  $D$ . From the control point of view, we consider Lipschitz curves  $t \mapsto q(t)$  tangent to  $D$ , called *horizontal curves*, and represented as solutions of:

$$\dot{q}(t) = \sum_{i=1}^m u_i(t) F_i(q(t)) = F(q(t), u(t))$$

where  $u = (u_1, \dots, u_m)^\top$  is the control. The length of an horizontal curve is given by:

$$l(q) = \int_0^T (u(t)^\top S(q(t))u(t))^{1/2} dt$$

where  $S$  is a symmetric matrix defined by  $g$ . The associated energy is:

$$E(q) = \int_0^T u(t)^\top S(q(t))u(t) dt.$$

Taking  $q_0, q_1 \in U$ , the SR-distance between  $q_0, q_1$  is defined as:

$$d_{SR}(q_0, q_1) = \inf\{l(\gamma); \gamma \text{ horizontal curve in } U \text{ joining } q_0 \text{ to } q_1\}.$$

This leads to the optimal control problem:

$$\min_{u(\cdot)} l(q), \quad \dot{q}(t) = F(q(t), u(t)).$$

The *Maupertuis principle* states that the length minimization problem is equivalent to the *energy minimization* problem:

$$\min_{u(\cdot)} E(q), \quad \dot{q}(t) = F(q(t), u(t)).$$

We can choose (locally) an orthonormal frame  $\{F_1, \dots, F_m\}$  for the distribution  $D$  so that  $S = \text{Id}$ , which from the control point of view means to apply a *feedback*  $u = \beta(q)v$  where  $\beta$  is a (smooth) invertible matrix.

Candidates as minimizers can be selected using the Maximum principle [37] which we recall in the next section and which we apply to our minimization problems.

### 3.2 Maximum principle

We refer the reader to [43] for a complete presentation. For our purpose, we need the following framework.

#### 3.2.1 Optimal control formulation and geometric concepts

We introduce  $\tilde{q} = (q, q^0)$  and we consider the (cost) extended system:

$$\begin{aligned} \dot{q} &= F(q, u), \\ \dot{q}^0 &= \sum_{i=1}^m u_i^2 = L(q, u), \\ q^0(0) &= 0. \end{aligned}$$

The associated optimal control problem is the *Mayer problem*:

$$\min_{u \in \mathcal{U}} h(\tilde{q}(T)),$$

where  $h$  is a (smooth) function,  $T$  is the fixed transfer time and the set of admissible controls  $\mathcal{U}$  is the set  $L^\infty([0, T])$  of bounded measurable mappings taking their values in  $L^\infty([0, T])$ . Additionally we impose boundary conditions of the form:

$$(\tilde{q}(0), \tilde{q}(T)) \in K$$

where  $K$  is a closed subset of  $\mathbb{R}^{n+1} \times \mathbb{R}^{n+1}$ .

We denote by  $t \mapsto \tilde{q}(t, \tilde{q}(0), u)$  the solution associated to the control  $u(\cdot)$  and initiated from  $(q_0, 0)$ , and we assume it is defined on  $[0, T]$ . The *extremity mapping* is defined as the map:  $E : u(\cdot) \in \mathcal{U} \mapsto \tilde{q}(T, \tilde{q}(0), u)$  where  $T, \tilde{q}(0)$  are fixed. The image of  $E$  is the *accessibility set*:  $A(\tilde{q}(0), T) = \bigcup_{u \in \mathcal{U}} \tilde{q}(T, \tilde{q}(0), u)$ .

Next we recall the necessary optimality conditions associated to the Mayer problem.

### 3.2.2 Weak Maximum principle and transversality conditions

*Extremality conditions.* The first conditions express the fact that the solution  $\tilde{q}(T)$  associated to a minimizing control  $u(\cdot)$  belongs to the boundary of the accessibility set and corresponds to a singularity of the extremity mapping. The result in the optimal control theory literature is known as the weak Maximum Principle [14] and is an Hamiltonian formulation of the Lagrange multiplier rule in the classical calculus of variations [10].

**Proposition 1** *If  $(u(\cdot), q(\cdot))$  is a control-trajectory minimizer on  $[0, T]$ , then there exist  $\tilde{p} = (p, \lambda_0) \in \mathbb{R}^n \times \mathbb{R} \setminus 0$  such that the (absolutely continuous) curve  $t \mapsto z(\cdot) = (q(\cdot), p(\cdot))$  satisfies a.e. the equations:*

$$\dot{q} = \frac{\partial H}{\partial p}(z, u), \quad \dot{p} = -\frac{\partial H}{\partial q}(z, u), \quad \frac{\partial H}{\partial u} = 0$$

where  $H(z, u) = \langle p, F(q, u) \rangle + \lambda_0 L(q, u)$ ,  $\lambda_0$  being a constant.

**Definition 3**  *$H(z, u)$  is called the pseudo-Hamiltonian and  $\tilde{p} = (p, \lambda_0) \neq (0, 0)$  is the (cost extended) adjoint vector. A trajectory-control pair  $(z, u)$  is called an extremal and its projection  $q$  on the state space is called a geodesic.*

*Boundary conditions.* We also have that boundary conditions associated to the Mayer problem imply that:

$$(\tilde{p}(0), -\tilde{p}(T)) \in \lambda \nabla_{\tilde{q}} h(\tilde{q}(T)) + N_K(\tilde{q}(0), \tilde{q}(T)) \quad (7)$$

where  $N_K$  is the (limiting) normal cone to  $K$  and  $\lambda \geq 0$ .

**Definition 4** *Condition (7) is called the transversality condition. An extremal satisfying the boundary conditions and the transversality condition is called a BC-extremal.*

### 3.2.3 Application to the micro-swimmers.

Notice first that according to the weak maximum principle, we have two types of distinct extremals in SR-geometry.

*Normal case.* If  $\lambda_0 \neq 0$ , it can be normalized to  $-1/2$  (corresponding to minimizing the energy). Introducing  $H_i(q, p) = \langle p, F_i(q) \rangle$  and using  $\frac{\partial H}{\partial u} = 0$ , we obtain  $u_i = H_i(q, p)$ . Substituting back this expression for these extremal controls into the pseudo-Hamiltonian  $H$  gives the (*true*) normal Hamiltonian  $H_n(q, p) = 1/2 \sum_{i=1}^m H_i^2(q, p)$ . The corresponding extremals solution of  $\overrightarrow{H}_n = \left( \frac{\partial H}{\partial p}, -\frac{\partial H}{\partial q} \right)$  are called normal and their  $q$ -projections are called normal geodesics.

*Abnormal case.* If  $\lambda_0 = 0$ , the associated extremal control is defined by the (implicit) relations  $H_i(q, p) = 0$ ,  $i = 1, \dots, m$ . The corresponding extremals are called abnormal and their  $q$ -projections are called abnormal geodesics. A normal geodesic is called strict if it is not the projection of an abnormal geodesic.

*Geometric remark.* The abnormal extremals correspond to singularities of the extremity mapping associated to the control system  $\dot{q} = F(q, u)$  and do not depend on the cost.

*Transversality conditions.* For the micro-swimmers we have two applications:

- *Periodicity.* This is expressed as  $\theta(0) = \theta(T)$  and it leads to the condition:

$$p_\theta(0) = p_\theta(T) \quad (8)$$

to produce a *smooth* stroke.

- *Efficiency maximization.* As a consequence of the Maupertius principle, and assuming that  $x_0(0) = 0$ , we can suppose that the efficiency is expressed as  $\mathcal{E}' = x_0(T)^2/E(\gamma)$  for a given stroke  $\gamma$ . If  $h = -x_0(T)/q^0(T)$ , then the transversality condition (7) becomes:

$$(p_0, \lambda_0) = \lambda \frac{\partial h}{\partial (x_0, q^0)} \quad (9)$$

at the final point  $(x_0(T), q^0(T))$ .

This has the following interpretation: at the final point, the adjoint vector is normal to the level set  $h = c$ , where  $c$  is the maximal efficiency.

### 3.2.4 Chow and Hopf-Rinow theorems

**Proposition 2** *Let  $D_{L.A.}$  be the Lie algebra generated by  $\{F_1, \dots, F_m\}$  and assume that the following rank condition hold:  $\{\forall q \in U, \dim D_{L.A.}(q) = n, (U \simeq \mathbb{R}^n)\}$ . Then:*

- 1 *For each  $q_0, q_1 \in U$  there exists a piecewise smooth horizontal curve joining  $q_0$  to  $q_1$  corresponding to a piecewise constant control.*
- 2 *Sufficiently near points  $q_0, q_1 \in U$  can be joined by a minimizing geodesic.*

*Application* The first assertion is known as Chow's theorem and can be found in [33]. Assuming the micro-swimmer starts at  $q(0) = (x_0(0), \theta(0))$  and that we fix the desired displacement to  $x_0(T) = x_d$  in  $U$ . Then, there exists a piecewise constant control such that the micro-swimmer can reach the configuration  $(x_d, \theta(0))$ . By construction this produces a closed curve in the  $\theta$ -space where  $T$  is a period (not necessary minimal). The second assertion is a local version of the standard Hopf-Rinow existence theorem. It can be easily globalized under standard (completeness) assumptions. Hence in our study we can restrict our analysis to (normal and abnormal) geodesic curves. The existence theorem is easily deduced when dealing with the maximal efficiency. Indeed, our state domain is bounded by the triangle  $\mathcal{T}$  and a direct computation shows that for strokes with "small amplitudes", the efficiency goes to zero with the amplitude  $A$ . A straightforward computation demonstrates that the triangle stroke corresponds to a low efficiency. Therefore, there exists a solution of the problem of maximizing efficiency.

### 3.2.5 Spheres with small radii and nilpotent approximations.

**Definition 5** The SR-sphere of center  $q_0$  with radius  $r$  is denoted by  $S(q_0, r) = \{q; d_{SR}(q_0, q) = r\}$ .

An important result in SR-geometry is the construction of the so-called *privileged coordinates* to estimate the size of the sphere with small radius [27, 7].

**Definition 6** Let  $D_1 = \text{span}\{F_1, \dots, F_m\}$ , we define recursively  $D_k = D_{k-1} + \text{span}\{[D_1, D_{k-1}]\}$  with  $n_k(q_0)$  be the rank of  $D_k$  at  $q_0$ . Assume that the rank condition holds:  $\dim D_{L.A.}(q_0) = n (= \dim T_{q_0}U)$  for each  $q_0$ . Consider the flag  $D_1(q_0) \subset D_2(q_0) \subset \dots \subset D_{n_r}(q_0) = D_{L.A.}(q_0)$ . Then  $n_r(q_0)$  is called the degree of non-holonomy and the sequence  $(n_1(q_0), \dots, n_r(q_0))$  is called the growth vector of the distribution  $D$  at  $q_0$ .

Using [27], we introduce the following notions.

**Definition 7** Let  $q_0 \in U$  and let  $f$  be a germ of smooth function at  $q_0$ . The multiplicity of  $f$  at  $q_0$  is the number defined by:

- $\mu(f) = \min \{k, | \exists X_1, \dots, X_k \in D \text{ such that } L_{X_1}, \dots, L_{X_k} f(q_0) \neq 0 \}$  where  $L_X f$  denotes the Lie derivative of  $f$  w.r.t.  $X$ :  $L_X f = \frac{\partial g}{\partial q} \cdot X(q)$ .
- if  $f(q_0) \neq 0$ ,  $\mu(f) = 0$  and  $\mu(0) = +\infty$ .

**Definition 8** Let  $f$  be a germ of smooth function at  $q_0$ ,  $f$  is called privileged at  $q_0$  if  $\mu_f = \min \{k; df_{q_0}(D^k(q_0)) \neq 0\}$ .

A coordinate system  $(q_1, \dots, q_n)$  defined on an open subset of  $U$  at  $q_0$ , identified to 0, is called privileged if the coordinates functions  $q_i$ ,  $i = 1 \leq i \leq n$  are privileged at  $x_0$ . If  $w_i$  is the weight of  $q_i$  at  $q_0 = 0$ , the induced weight of  $\frac{\partial}{\partial q_i}$  is  $-w_i$ , and the weight of the dual variable  $p_i$  in  $T^*U$  is  $-w_i$ .

The following theorem can be found in [7].

**Theorem 1** *Let  $\{F_1, \dots, F_m\}$  be an orthonormal frame for the pair  $(D, g)$ . Fix  $q_0 \in U$  and let  $(q_1, \dots, q_n)$  be a privileged coordinates system at  $q_0 = 0$ , with weights  $w_1, \dots, w_n$ . Then, one can expand  $F_i$  as  $\sum_{j \geq -1} F_i^j$ , where  $F_i^j$  are homogeneous vector fields (for the weight systems) with degree  $\geq -1$ . Denoting  $\hat{F}_i = F_i^{-1}$ , the family  $\hat{F}_i$  generates a nilpotent Lie algebra with similar growth vector (at  $q_0 = 0$ ). Moreover, for small  $q$  it gives the following estimate of the SR-distance:  $B(|q_1|^{1/w_1} + \dots + |q_n|^{1/w_n}) \leq d_{SR}(0, q) \leq A(|q_1|^{1/w_1} + \dots + |q_n|^{1/w_n})$ , where  $A, B$  are constants.*

3.2.6 Singularities of SR-spheres with small radius.

**Definition 9** *Let  $H_n(q, p) = 1/2 \sum_{i=1}^m H_i^2(q, p)$  the normal Hamiltonian and let  $\exp t\vec{H}_n$  denote the local-one parameter group associated to  $\vec{H}_n$  with  $\Pi : (q, p) \mapsto q$  be the standard projection. Assume  $q_0$  is fixed, the exponential mapping is given by the map:  $\exp_{q_0} : (t, p) \mapsto \Pi \left( \exp t\vec{H}_n(q_0, p) \right)$ .*

**Definition 10** *Let  $\gamma(\cdot)$  be a reference (normal or abnormal) geodesic defined on  $[0, T]$ . The time  $t_c$  is called the cut time if  $\gamma$  is optimal up to  $t_c$  but no longer optimal for  $t > t_c$ , and  $q(t_c)$  is called the cut point. Considering all geodesics starting from  $q_0$ , the set of cut points forms the cut locus denoted by  $C_{cut}(q_0)$ . The time  $t_{1c}$  is called the first conjugate time if the reference geodesic  $\gamma$  is optimal up to  $t_{1c}$  and no longer optimal for  $t > t_{1c}$  for the  $C^1$ -topology on the set of horizontal curves, and the point  $\gamma(t_{1c})$  is called the first conjugate point. The set of first conjugate points calculated over all geodesics forms the (first) conjugate locus and is denoted by  $C(q_0)$ .*

Conjugate points can be computed (under suitable assumptions) in the normal and abnormal case. In our study, we can restrict the analysis to the normal case and we have.

**Proposition 3** *Let  $\gamma(\cdot)$  be a strict normal geodesic defined on  $[0, T]$ . Then, the first conjugate time  $t_{1c}$  is the first time  $t$  such that the exponential mapping  $\exp_{\gamma(0)}$  is not of full rank  $n$ . This is equivalent to the existence of a Jacobi field  $J(t) = (\delta q(t), \delta p(t))$  solution of the Jacobi equation:*

$$\delta z(t) = \frac{\partial}{\partial z} \left[ \vec{H}_n(\gamma(t)) \right] \delta z(t)$$

which is vertical at time  $t=0$  and  $t=t_{1c}$ , i.e.  $\delta q(0) = \delta q(t_{1c}) = 0$ .

A property of SR-geometry is the following.

**Proposition 4** *There exist conjugate points arbitrarily closed to  $q_0$ , and a consequence is that SR-spheres with arbitrary small radius have singularities.*

### 3.3 SR-geometry in dimension 3

Motivated by our micro-swimmer study, in this section we recall refined results related to singularities of three-dimensional SR-spheres with small radius, that is explicit conjugate and cut loci computation. Those results are the consequence of

intense research activities in SR-geometry at the end of the nineties, see [19] for the contact case and [1] for the Martinet case. Here  $U$  is assumed to be a neighbourhood of  $q_0$  identified to 0, and  $(D, g)$  is defined by the choice of an orthonormal frame  $\{F_1, F_2\}$ . The distribution can be represented as  $D = \ker \omega$ , where  $\omega$  is a well-defined (up to a factor) one-form.

A first geometric result comes from [46].

### 3.3.1 Local one-form models.

Introducing  $q = (x, y, z)$ , we have that the only *stable models* are given by:

- *Contact-Darboux case* (Dido). In this case, the normal form is expressed as:

$$\omega = dz + (x dy - y dx).$$

- *Martinet case*. The normal form is:

$$\omega = dz - \frac{y^2}{2} dx.$$

### 3.3.2 Associated (graded) local model of SR-metric.

*Geometry.* Near the origin, the SR-model is represented by an affine control system:

$$\frac{dq}{dt} = u_1 F_1(q) + u_2 F_2(q),$$

and we minimize the energy:

$$\min_{u(\cdot)} \int_0^T (u_1^2(t) + u_2^2(t)) dt.$$

The (pseudo) group  $\mathcal{G}$  defining the geometry is induced by the following actions:

- local diffeomorphisms  $Q = \varphi(q)$  preserving zero,
- feedback  $u = \beta(q)v$  where  $\beta(q)$  is restricted to the orthogonal group  $O(2)$  (so that  $u_1^2 + u_2^2 \mapsto v_1^2 + v_2^2$ ).

The (normal) geodesic flow is defined by the Hamiltonian  $H_i(q, p) = \langle p, F_i(q) \rangle$ ,  $i = 1, 2$ . A local diffeomorphism  $\varphi$  can be lifted into the *Mathieu symplectomorphism*  $\vec{\varphi}$  defined as:

$$Q = \varphi(q), \quad p^\top = \frac{\partial \varphi^\top}{\partial q} P^\top.$$

Reducing the actions of  $g \in \mathcal{G} = (\varphi, \beta)$  to the action of  $\vec{\varphi}$  on an Hamiltonian (function)  $H$  to:

$$g \cdot H = H \circ \vec{\varphi}$$

we obtain the following, see [12].



**Theorem 2** *The following diagram is commutative:*

$$\begin{array}{ccc}
 \{F_1, F_2\} & \xrightarrow{\lambda} & \frac{1}{2} (H_1^2 + H_2^2) \\
 \mathcal{G} \downarrow & \curvearrowright & \downarrow \mathcal{G} \\
 \{F_1^*, F_2^*\} & \xrightarrow{\lambda} & \frac{1}{2} (H_1^{2*} + H_2^{2*})
 \end{array}$$

(It is equivalent to say that  $\lambda$  is covariant).

A normal form is a section on the set of orbits for the  $\mathcal{G}$ -actions, and Theorem 2 states that it can be performed either on the set of SR-metrics or on the set of (normal) Hamiltonians.

A standard method in singularity theory [31] is to *linearize* the calculations by working on the jet spaces and restricting to homogeneous transformations. This can be also be performed using a *graded* system of coordinates as the privileged coordinates in SR-geometry to obtain graded normal forms. Different algorithms exist in the literature, see [19] for the contact case, and [1] for the Martinet case.

We recall the results in the contact and Martinet case.

- *Contact case.*  $q = (x, y, z)$  are the privileged coordinates where  $x, y$  are of weight 1 and  $z$  is of weight 2.

- ★ *Nilpotent model.* (Heisenberg-Brockett-Dido). This is a model of order  $-1$  (Dido form) and it is given by the orthonormal frame:

$$\hat{F}_1 = \frac{\partial}{\partial x} + y \frac{\partial}{\partial z}, \quad \hat{F}_2 = \frac{\partial}{\partial y} - x \frac{\partial}{\partial z}.$$

- ★ *Model of order zero.* Keeping all the terms of order  $\leq 0$ , we have Theorem 3.

**Theorem 3** ([17]) *In the contact case, the model of order 0 is similar to the model of order  $-1$ .*

- ★ *Model of order 1.* Keeping the terms of order  $\leq 1$ , the model in [19] is given by:

$$F_1 = \hat{F}_1 + yQ(w) \frac{\partial}{\partial z}, \quad F_2 = \hat{F}_2 - xQ(w) \frac{\partial}{\partial z}$$

with  $w = (x, y)$  and  $Q$  is a quadratic form:  $Q = \alpha x^2 + 2\beta xy + \gamma y^2$  where  $\alpha, \beta, \gamma$  are parameters.

*Geodesics equations.* Let us first analyze the Dido model. Recall that the Lie brackets of two (smooth) vector fields  $F, G$  defined on  $U$  is computed with the convention:

$$[F, G](q) = \frac{\partial F}{\partial q}(q)G(q) - \frac{\partial G}{\partial q}(q)F(q)$$

and the Poisson bracket of two Hamiltonians  $P_1, P_2$  is given by

$$\{P_1, P_2\}(q, p) = dP_1(\overrightarrow{P_2})(q, p).$$

If  $H_F(q, p) = \langle p, F(q) \rangle$ ,  $H_G(q, p) = \langle p, G(q) \rangle$  one has  $\{H_F, H_G\}(q, p) = \langle p, [F, G](q) \rangle$ .

To compute the geodesics in the *Heisenberg-Brockett-Dido case* we complete  $F_1 = \hat{F}_1, F_2 = \hat{F}_2$  by  $F_3 = \frac{\partial}{\partial z}$  to form a frame. We denote  $H_i(q, p) = \langle p, F_i(q) \rangle$ ,  $i = 1, 2, 2$  and instead of the symplectic coordinates  $(x, y, z, p_x, p_y, p_z)$  we use  $(x, y, z, H_1, H_2, H_3)$ .

The geodesic dynamics is given by  $\dot{x} = H_1, \dot{y} = H_2, \dot{z} = H_1 y - H_2 x$  and we have  $[F_1, F_2](q) = 2F_3(q)$ . Hence

$$\begin{aligned} \dot{H}_1 &= dH_1\left(\frac{1}{2}(H_1^2 + H_2^2)\right) = \{H_1, H_2\}H_2 \\ &= 2H_2H_3, \\ \dot{H}_2 &= -2H_1H_3, \\ \dot{H}_3 &= 0, \end{aligned}$$

since the Lie brackets of length  $\geq 3$  are zero.

Integration. We have that  $H_3(t)$  is constant and by introducing  $H_3 = p_z = \lambda/2$  we obtain the equation of the linear pendulum  $\ddot{H}_1 + \lambda^2 H_1 = 0$ . The equations are integrable by quadratures using trigonometric functions. The integration is straightforward if we observe that:

$$\ddot{z} - \frac{\lambda}{2} \frac{d}{dt}(x^2 + y^2) = 0.$$

Micro-local description. Taking  $q(0) = 0$ , we have that:

- $\lambda = 0$ . In this case  $z = 0$  and the geodesics contained in the plane  $(x, y)$  are lines.
- $\lambda \neq 0$ . An easy integration shows that in that case the geodesics are given by:

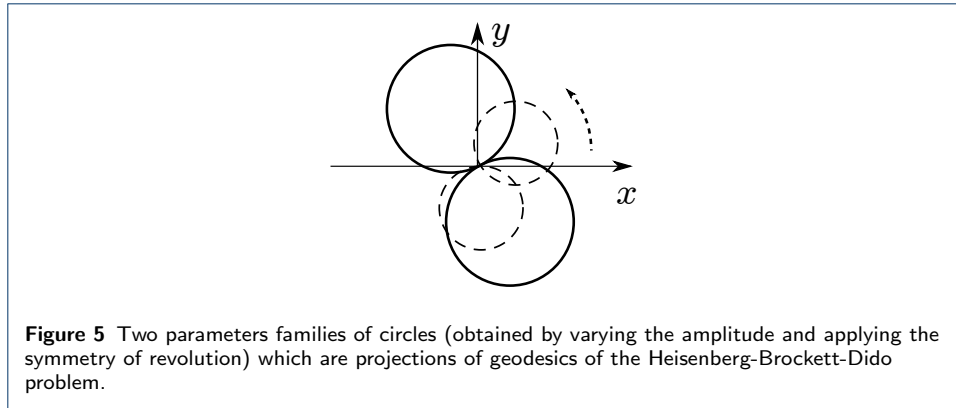
$$\begin{aligned} x(t) &= \frac{A}{\lambda} (\sin(\lambda t + \phi) - \sin \phi) \\ y(t) &= \frac{A}{\lambda} (\cos(\lambda t + \phi) - \cos \phi) \\ z(t) &= \frac{A^2}{\lambda} t - \frac{A^2}{\lambda^2} \sin(\lambda t) \end{aligned} \tag{10}$$

with  $A = \sqrt{H_1^2 + H_2^2}$  and  $\phi$  is the angle of the vector  $(\dot{x}, -\dot{y})$  at the origin.

In particular we can deduce the following geometric properties.

### Proposition 5

- (1) All the controls for  $\lambda \neq 0$  are periodic with period  $2\pi/\lambda$ .
- (2) The corresponding  $(x, y)$  projections will form families of circles that are invariant by any rotation along the  $z$ -axis.



A family of projections is represented on Fig.5. Interpreting these geodesics as strokes for the micro-swimmer (and  $z$  is taken the displacement variable). The displacement associated to a stroke being given by  $dz = -2dx \wedge dy$  and is proportional to the standard volume form in  $\mathbb{R}^2$ . Conjugate and cut loci. They can be easily computed from (10) and according to [19] they can be calculated restricting the exponential mapping to the  $(x, y)$ -projection. We can prove the following proposition.

**Proposition 6** *If  $\lambda \neq 0$ , the first conjugate time occurs at  $2\pi/\lambda$  and corresponds to the cut point. Hence, it occurs exactly at the period and the projection of the cut locus in the  $(x, y)$ -plane degenerates into the origin.*

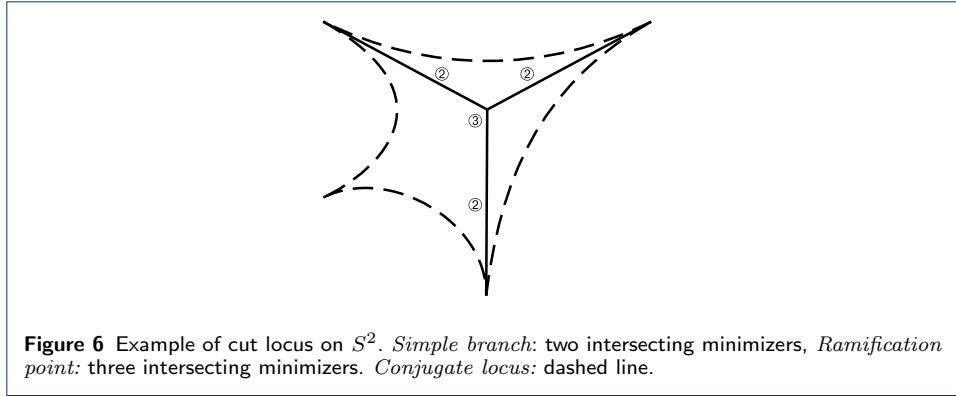
Generalized Dido case. Conjugate and cut loci computations in the small radius case where generalized in [2] and this study is relevant in our problem. The main features are the following. In the Dido problem, due to the  $z$ -symmetry of revolution the projection of the conjugate and cut loci in the  $(x, y)$ -plane is reduced to a single point. In the generalized Dido case, the SR-problem leads to compute conjugate and cut loci for Riemannian metrics on the sphere. This is related to the seminal result from [35].

**Theorem 4** *Let  $g$  be an analytic Riemannian metric on the 2-sphere  $S^2$ . Then the cut locus of a point is a finite tree, whose branches extremities are cusp points of the conjugate locus. Each ramification counts the number of intersecting minimizing geodesics.*

An example is represented on Fig.6.

- *Martinet case.* We use the classification from [14, 1]. We denote by  $q = (x, y, z)$  the privileged coordinates, and we have that  $x, y$  are of weight 1 and  $z$  is of weight 3. The distribution  $D$  is normalized to the Martinet form:  $\ker \omega$ ,  $\omega = dz - y^2/2 dx$ .

Geometric meaning. The distribution is given by  $D = \text{span}\{F_1, F_2\}$  with  $F_1 = \frac{\partial}{\partial x} + \frac{y^2}{2} \frac{\partial}{\partial z}$ ,  $F_2 = \frac{\partial}{\partial y}$ . We have  $[F_1, F_2](q) = 2y \frac{\partial}{\partial z}$ . Hence  $[F_1, F_2](q) \in D(q)$  for  $y = 0$  and the plane  $y = 0$  is called the *Martinet surface*. Abnormal curves are



defined by  $H_1 = H_2 = 0$  with  $H_i(q, p) = \langle p, F_i \rangle$ ,  $i = 1, 2$ . Differentiating, one gets for  $y = 0$ ,

$$\begin{aligned} H_1 = H_2 = \{H_1, H_2\} &= 0 \\ u_1 \{\{H_1, H_2\}, H_1\} + u_2 \{\{H_1, H_2\}, H_2\} &= 0 \end{aligned} \quad (11)$$

An easy calculation shows that:

$$[[F_1, F_2], F_1] = 0, \quad [[F_1, F_2], F_2] = 2 \frac{\partial}{\partial z}.$$

Hence we obtain the following result.

**Proposition 7** *In the normal form, the abnormal curves are contained in the Martinet surface and are lines parallel to the  $x$ -axis. Starting from the origin  $(0, 0, 0)$ , it is given by the abnormal curve  $\gamma_a : t \mapsto (t, 0, 0)$ .*

The metric can be normalized to the (isothermal) form:  $g = a(q)dx^2 + b(q)dy^2$  and the mappings  $a(q), b(q)$  can be expanded using the following weight systems:

- *Model of order  $-1$*  (Martinet flat case). It corresponds to  $g = dx^2 + dy^2$ .
- *Model of order 0*. The metric is of the form  $g = (1+dy)^2 dx^2 + (1+\beta x + \gamma y)^2 dy^2$ .

The squares are introduced to simplify the geodesics computation, but at order 0 we have the approximations:

$$(1 + \alpha y)^2 \sim 1 + 2\alpha y, \quad (1 + \beta x + \gamma y)^2 \sim 1 + 2\beta x + 2\gamma y.$$

Geodesic equations: order 0. We introduce the orthonormal vector fields:

$$G_1 = F_1/\sqrt{a}, \quad G_2 = F_2/\sqrt{b}$$

which we complete with  $G_3 = \frac{\partial}{\partial z}$  to form a frame. Using the notation  $H_i(q, p) = \langle p, G_i(q) \rangle$ ,  $i = 1, 2, 3$  the normal extremals are solutions of:

$$\begin{aligned} \dot{x} &= \frac{H_1}{\sqrt{a}}, \quad \dot{y} = \frac{H_2}{\sqrt{b}}, \quad \dot{z} = \frac{y^2 H_1}{2\sqrt{a}}, \\ \dot{H}_1 &= \frac{H_2}{\sqrt{ab}} \left( y H_3 - \frac{\partial a}{\partial y} \frac{1}{2\sqrt{a}} H_1 + \frac{\partial b}{\partial x} \frac{1}{2\sqrt{b}} H_2 \right), \\ \dot{H}_2 &= -\frac{H_1}{\sqrt{ab}} \left( y H_3 - \frac{\partial a}{\partial y} \frac{1}{2\sqrt{a}} H_1 + \frac{\partial b}{\partial x} \frac{1}{2\sqrt{b}} H_2 \right), \\ \dot{H}_3 &= 0. \end{aligned} \tag{12}$$

In particular, we have  $H_3 = p_z$  is constant (isoperimetric situation). Using the normal form of order 0, we can deduce the following proposition.

**Proposition 8**

- (1) If  $\beta = 0$ ,  $x$  is an additional cyclic coordinate and the geodesic flow is Liouville integrable.
- (2) The abnormal geodesic  $\gamma_a : t \mapsto (t, 0, 0)$  is strict if and only if  $\alpha \neq 0$ . If  $\alpha = 0$ , it is solution of (12) for each choice of  $p_z = H_3 = \lambda$ .

Pendulum equation. The geodesic equations are related to the pendulum equation. Indeed, parameterizing by arc-length gives  $H_1 = \cos \theta$ ,  $H_2 = \sin \theta$ . Setting  $H_3 = p_z = \lambda \neq 0$ , if  $\theta \neq k\pi$ , we get using (12):

$$\dot{\theta} = \frac{1}{\sqrt{a}\sqrt{c}} (y\lambda - \alpha \cos \theta + \beta \sin \theta).$$

Using the time reparameterization:

$$\sqrt{ac} \frac{d}{dt} = \frac{d}{d\tau}$$

and denoting by  $\phi'$  the derivative of a function  $\phi$  with respect to  $\tau$ , we can show that  $\theta$  is a solution of the equation:

$$\begin{aligned} \theta'' + \lambda \sin \theta + \alpha^2 \sin \theta \cos \theta \\ - \alpha \beta \sin^2 \theta + \beta \theta' \cos \theta = 0. \end{aligned} \tag{13}$$

Integrable case. If  $\beta = 0$ , the system is integrable and leads to a type of a (conservative) pendulum equation:

$$\frac{1}{2} \dot{\theta}^2 - \lambda \cos \theta - \frac{\alpha^2 \cos(2\theta)}{2} = E \tag{14}$$

where  $E$  is a constant. If  $\alpha = 0$ , (14) reduces to the standard pendulum equation. We refer the reader to [1, 14], for a detailed analysis but we can deduce already some geometric fact about the Martinet case versus the contact case of order zero.

In the Martinet case, there are many micro-local different geodesics, in particular if  $\beta = 0$  we can have the oscillating or rotating cases in the pendulum equations. To

parameterize the geodesics in this case, we need at least the complexity of *elliptic functions* [28] and only a small number of specific geodesics can be parametrized by periodic controls. In particular, it is related to *the Euler elastica* [26] to parameterize strokes for the micro-swimmers. Indeed, besides the simple strokes related to the linear pendulum, we can construct *eight shapes strokes* corresponding to Bernoulli lemniscates.

#### 4 Application: geometric and numerical study of the copepod swimmer.

The aim of this section is to provide a complete analysis of the copepod swimmer. We will start this section by introducing the numerical tools.

##### 4.1 Numerical methods

We use two sophisticated software recently developed to analyze optimal control problems.

- **Bocop**. The so-called direct approach transforms the infinite dimensional control problem into a finite dimensional problem. This is done by a discretization in time, applied to the state and control variables. Direct methods are usually less precise than indirect methods which are based on the Maximum Principle, but more robust with respect to the initialization. It can be used to initialize an indirect method. In the swimmer problem the **Bocop**'s software allows us to account for the triangle state constraints and to generate a stroke with large amplitude in the triangle interior.
- **HamPath**. This software is based upon indirect methods: in a nutshell, the Maximum Principle leads to a *shooting equation* which is implemented using either simple or multiple shootings. It is complemented by discrete or differential continuation (homotopy) methods to evaluate the solution, when starting initially from a known solution. In our case, it can be done with the **Bocop** software starting from strokes with large amplitude or by the mathematical evaluations of stroke of small amplitudes using nilpotent SR-models. This software uses the Jacobi fields to compute the differential of the shooting equation and is suitable to check second order necessary optimality conditions corresponding to conjugate points computation.

##### 4.2 Lie brackets and geodesics computation

The system is written as

$$\dot{q}(t) = \sum_{i=1}^2 u_i(t) F_i(q(t))$$

with  $q = (x_0, \theta_1, \theta_2)$ , and

$$F_i = \frac{\sin(\theta_i)}{\Delta(\theta)} \frac{\partial}{\partial x_0} + \frac{\partial}{\partial \theta_i}, \quad i = 1, 2$$

where  $\Delta(\theta) = 2 + \sin^2 \theta_1 + \sin^2 \theta_2$ . The metric is represented as

$$L(u_1, u_2) = a(q)u_1^2 + 2b(q)u_1u_2 + c(q)u_2^2$$

which can be taken either as the Euclidean metric or as the mechanical energy. A straightforward calculation shows that:

$$[F_1, F_2](q) = f(\theta_1, \theta_2) \frac{\partial}{\partial x_0}$$

with

$$f(\theta_1, \theta_2) = \frac{2 \sin \theta_1 \sin \theta_2 (\cos \theta_1 - \cos \theta_2)}{\Delta^2(\theta)}. \quad (15)$$

Furthermore,

$$[[F_1, F_2], F_i] = \frac{\partial f}{\partial \theta_i} \frac{\partial}{\partial x_0}, \quad i = 1, 2.$$

We observe in particular that  $f$  vanishes on the edges of the triangle  $\mathcal{T} : 0 \leq \theta_1 \leq \theta_2 \leq \pi$ .

According to our terminology previously introduced, we have the following result.

**Proposition 9**

- 1 *All interior points of the triangle  $\mathcal{T}$  are contact points.*
- 2 *The triangle  $\mathcal{T}$  represents the only (piecewise smooth) abnormal stroke, and each point – vertices excluded – is a Martinet point. It is a geodesic triangle in the Euclidean case.*

The Maximum Principle minimizing the energy  $L$  leads to introduce the pseudo-Hamiltonian:

$$H(z, u) = \langle p, F_1(q)u_1 + F_2(q)u_2 \rangle - \frac{1}{2} L(u_1, u_2).$$

Solving  $\partial H / \partial u = 0$  with  $H_i(q, p) = \langle p, F_i(q) \rangle$  gives:

$$u_1 = \frac{cH_1 - bH_2}{ac - b^2}, \quad u_2 = \frac{aH_2 - bH_1}{ac - b^2}$$

and the normal Hamiltonian is:

$$H_n = \frac{1}{2} \frac{cH_1^2 - 2bH_1H_2 + aH_2^2}{ac - b^2} \quad (16)$$

In the Euclidean case it simplifies into:

$$H_n = \frac{1}{2} (H_1^2 + H_2^2).$$

The geodesics equations can be written in the coordinates  $(q, H)$ ,  $H = (H_1, H_2, H_3)$  and we complete the vector fields  $F_1, F_2$  with  $F_3 = \frac{\partial}{\partial x_0}$  to form a frame.

Assuming for instance that  $L(u_1, u_2) = u_1^2 + u_2^2$ , we obtain that:

$$\dot{H}_1 = (fH_3)H_2, \quad \dot{H}_2 = -(fH_3)H_1$$

with  $H_3 = p_{x_0}$  is a constant (isoperimetric case). These equations can be expressed in terms of the curvature of the shape geodesic:  $t \mapsto \theta(t)$ . Recall that  $u = (u_1, u_2) = (\dot{\theta}_1, \dot{\theta}_2) = (H_1, H_2)$ . If we parameterize the solutions by arc-length, it is equivalent to take  $H_1^2 + H_2^2 = 1$ . We introduce:

$$H_1 = \cos \psi, \quad H_2 = \sin \psi, \quad p_{x_0} = \lambda$$

and we get

$$\dot{\psi} = -\lambda f(\theta).$$

Taking a Serret-Frenet frame  $(T, N)$  associated to  $t \mapsto \theta(t)$  one has

$$\dot{\theta} = T, \quad \dot{T} = kN, \quad \dot{N} = -kT$$

and the curvature is given by

$$k = \dot{\theta}_1 \ddot{\theta}_2 - \dot{\theta}_2 \ddot{\theta}_1 = u_1 \dot{u}_2 - u_2 \dot{u}_1.$$

Since  $\psi = \arctan(H_2/H_1)$ , we obtain

$$\dot{\psi} = \dot{H}_2 H_1 - \dot{H}_1 H_2 = -k. \quad (17)$$

### 4.3 Numerical simulations and geometric comments in the copepod case

#### 4.3.1 Complexity of normal strokes

On Fig.8-9, we represent different types of strokes corresponding to the geodesics equations *without taking into account the state constraints* on the shape variables. In particular, we get the standard simple curves, limaçons as well as eight shaped curves but more complex shapes can also be found in the set of solutions. These curves are obtained using the `HamPath` software which also allows us to check the second order optimality conditions by computing conjugate points. From those simulations only the simple strokes have no conjugate points.

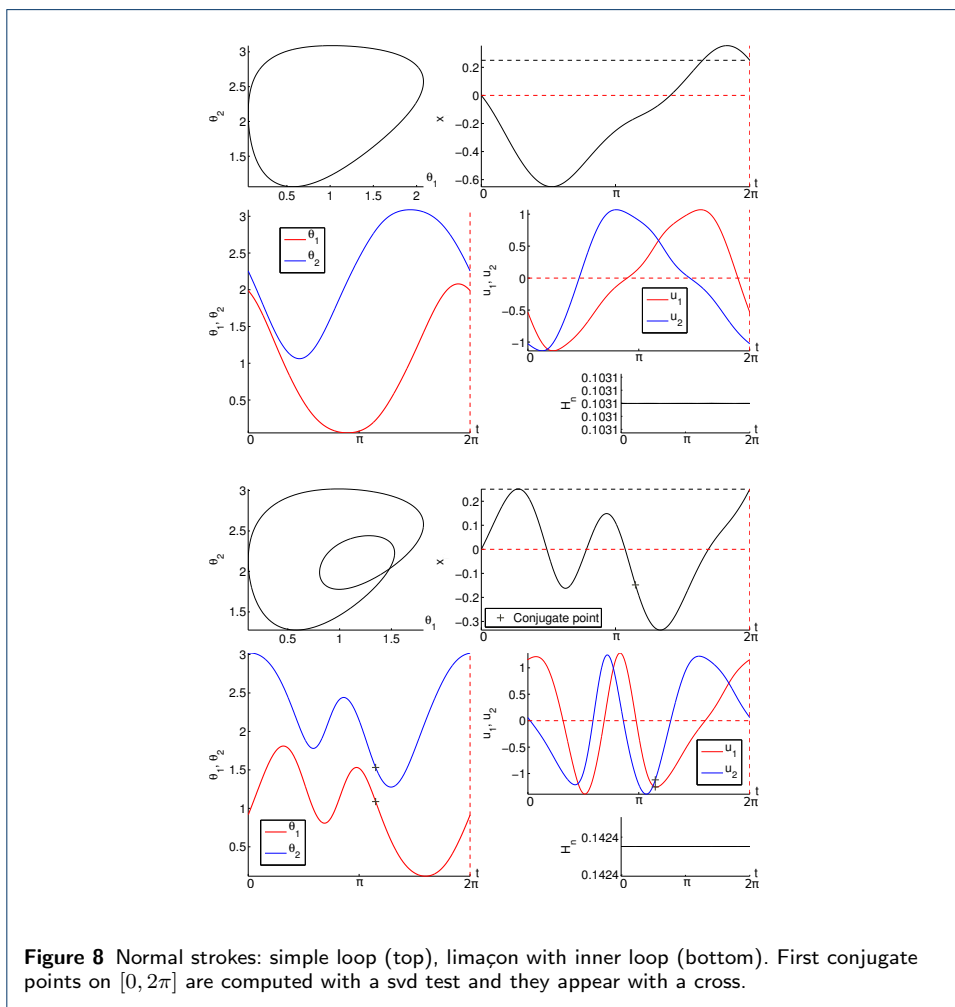
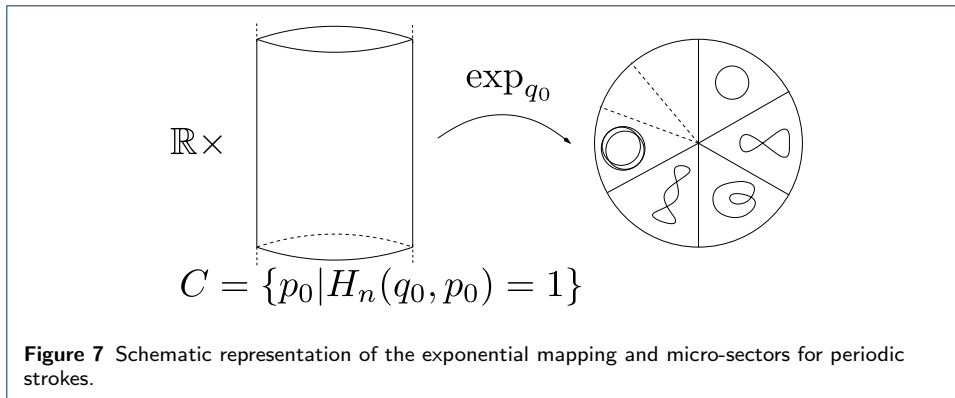
*Microlocal sectors* of the exponential mapping of the covering space are represented on Fig.7.

#### 4.3.2 Complexity of normal strokes constrained to the triangle $\mathcal{T}$

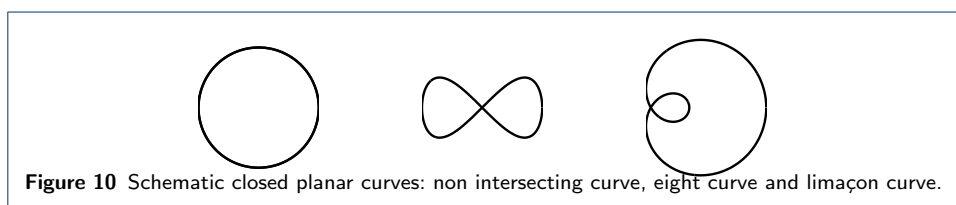
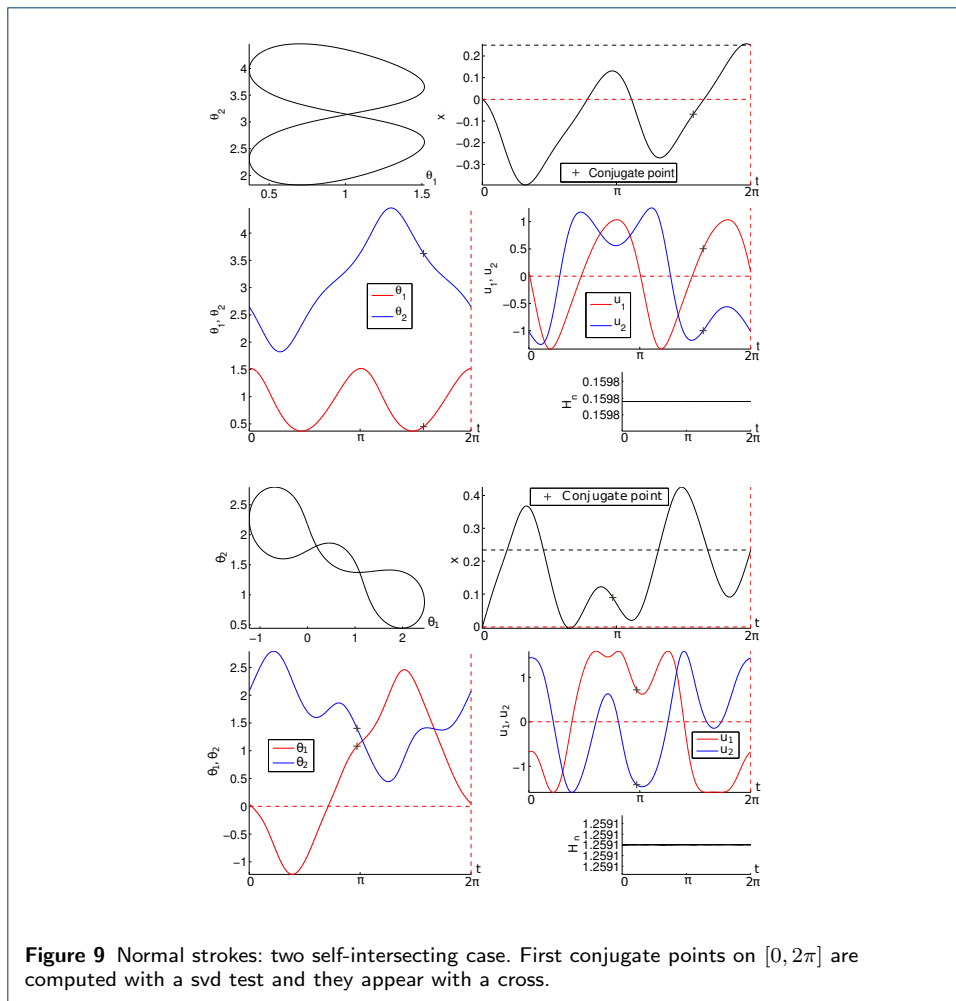
We represent on Fig.11 geodesics strokes resulting from calculations while taking into account the triangle constraint  $\mathcal{T} : 0 \leq \theta_1 \leq \theta_2 \leq \pi$ . Schematic periodic strokes with constraints are represented on Fig.10.

Fig.11 (top) displays a simple curve of large amplitudes obtained using the `Bocop` software. On Fig.12 the reader can see families of simple curves and limaçons obtained constrained to the interior of the triangle, as well as eight shape curves on the sides of the triangles. Using the `HamPath` software, we can proceed with the computation of conjugate points in each case. Conjugate points do appear for limaçons and eight curves.

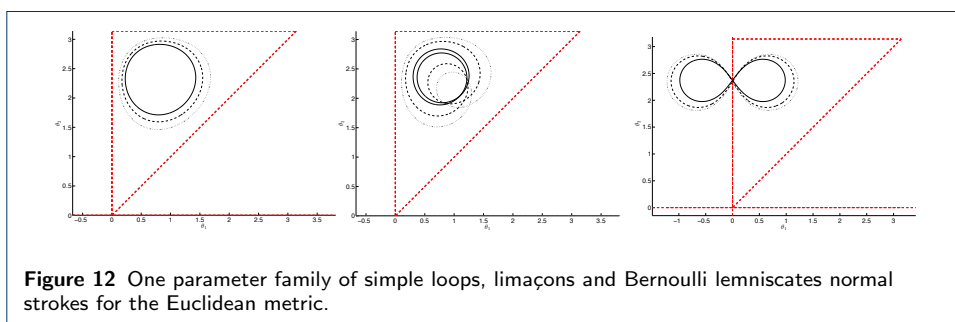
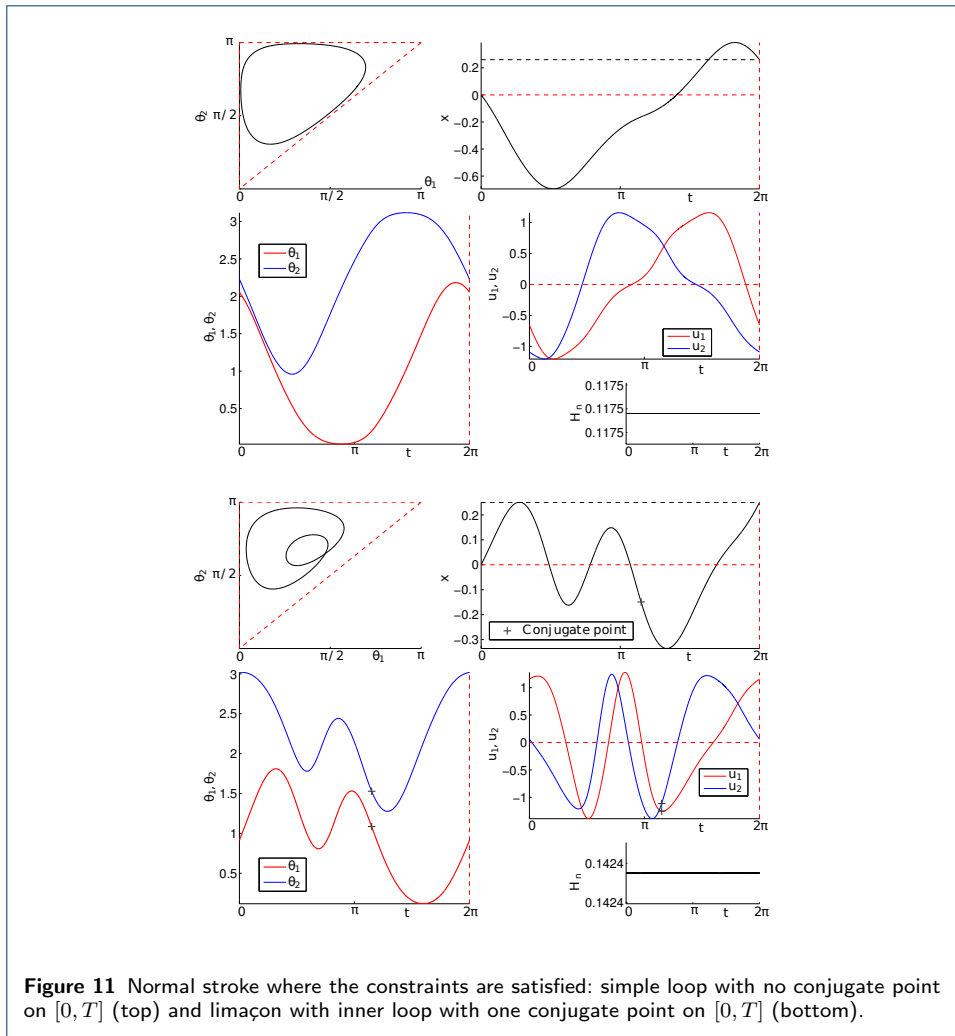




*Geometric explanation.* At an interior point of the triangle, simple strokes are predicted by the nilpotent model. A limaçon can occur also by perturbing a simple stroke *followed twice*, which is clear from the numerical simulation. Eight shaped curves can appear only on the sides of the triangle as predicted by the Bernoulli lemniscate associated to a periodic inflexional Euler elastica. Note also the role of the symmetry group  $\Sigma$  in the construction.



*Conjugate points computation.* The `HamPath` software allows to compute easily conjugate points. They appear for the limaçon and the eight shaped curves. Hence, simple closed curve are the only candidates as minimizers. This result is obtained as a numerical evidence of our approach versus using calculations based on Green's theorem. Note that for limaçons with small amplitude they are produced by perturbing a simple closed curve of the Dido model followed twice, and this gives a rigorous proof of the existence of a conjugate point since for the nilpotent model they appear exactly at the period.



#### 4.4 Numerical computation of the center of swimming strokes and SR-invariant computation in the copepod case

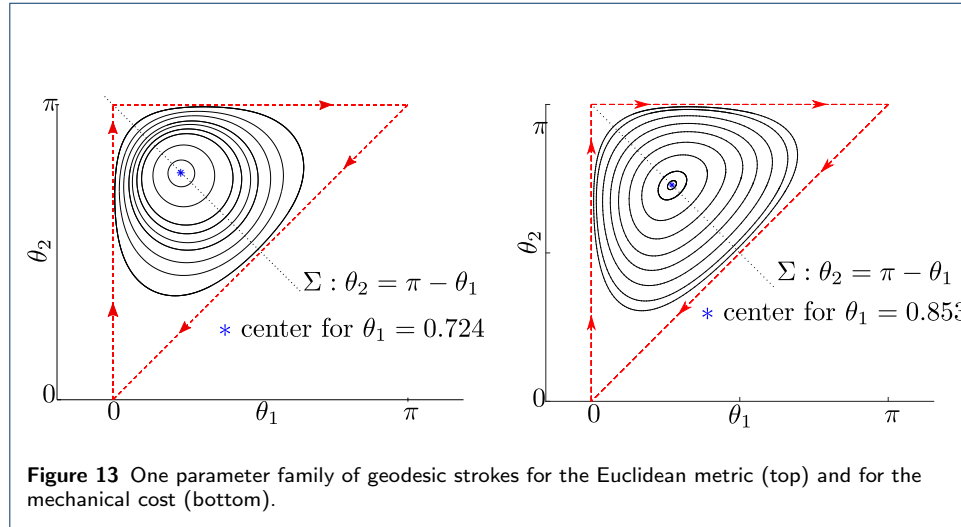
First, we need the following concept observed in numerical simulations and reminiscent of the so-called Lyapunov-Poincaré theorem in celestial mechanics [32].

**Definition 11** A center of swimming, denoted by  $C$ , is a point in the  $\theta$ -shape space from which we can observe a one parameter family  $\{\gamma_\lambda; \lambda \geq 0\}$  of simple strokes emanating from  $C$  which degenerates into  $C$  when  $\lambda \rightarrow 0$ . Moreover, we

impose that for  $\lambda$  small enough each of stroke in the one parameter family is length minimizing (for fixed displacement).

#### 4.4.1 Numerical simulations

We represent on Fig.13 numerical computations of centers of swimming for the copepod swimmer corresponding to the Euclidean metric case and for the mechanical energy cost case. In both cases, the centers of swimming are on the line



$\Sigma : \theta_2 = \pi - \theta_1$ , thanks to the symmetry of the geodesic flow with respect to the symmetry  $\sigma_3 : (\theta_1, \theta_2) \mapsto (\pi - \theta_2, \pi - \theta_1)$ .

In Tables 2 and 3 we represent the corresponding efficiency versus the efficiency of abnormal and limaçon strokes in the Euclidean and the mechanical case. Based on

Types of stroke	$x_0(T)$	$l(\gamma)$	$x_0(T)/l(\gamma)$
Simple loops	$5.50 \times 10^{-2}$	1.98	$2.52 \times 10^{-2}$
	$1.40 \times 10^{-1}$	3.79	$3.70 \times 10^{-2}$
	$1.70 \times 10^{-1}$	4.34	$3.92 \times 10^{-2}$
	$2.00 \times 10^{-1}$	4.95	$4.04 \times 10^{-2}$
	$2.10 \times 10^{-1}$	5.11	$4.11 \times 10^{-2}$
<b>Optimal stroke</b> Fig.15 (top)	<b><math>2.17 \times 10^{-1}</math></b>	<b>5.18</b>	<b><math>4.19 \times 10^{-2}</math></b>
	$2.20 \times 10^{-1}$	5.35	$4.11 \times 10^{-2}$
	$2.30 \times 10^{-1}$	5.62	$4.09 \times 10^{-2}$
	$2.50 \times 10^{-1}$	6.31	$3.97 \times 10^{-2}$
	$2.74 \times 10^{-1}$	9.05	$3.03 \times 10^{-2}$
Abnormal	$2.74 \times 10^{-1}$	10.7	$2.56 \times 10^{-2}$
Limaçon	$2.00 \times 10^{-1}$	6.15	$3.25 \times 10^{-2}$

**Table 2** Geometric efficiency for the abnormal stroke and different normal strokes with the Euclidean cost.

those tables, we display on Fig.15 the most efficient stroke for the copepod swimmer in both cases and we check numerically that it corresponds to the optimal solution using the transversality condition of the Maximum Principle.

In Fig.16 the efficiency curve for the mechanical energy is represented for the normal strokes and can be compared with the efficiency of the abnormal stroke.

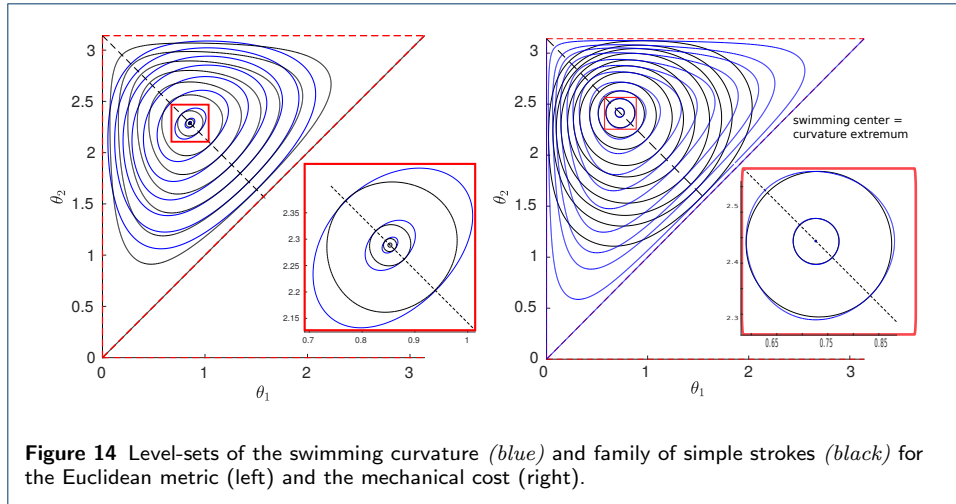


**Figure 14** Level-sets of the swimming curvature (blue) and family of simple strokes (black) for the Euclidean metric (left) and the mechanical cost (right).

Types of strokes	$x_0(T)$	$l(\gamma)$	$x_0(T)/l(\gamma)$
Simple loops	$0.50 \cdot 10^{-1}$	0.994	$5.03 \times 10^{-2}$
	$1.50 \cdot 10^{-1}$	1.86	$8.06 \times 10^{-2}$
	$1.70 \times 10^{-1}$	2.02	$8.41 \times 10^{-2}$
	$2.00 \times 10^{-1}$	2.28	$8.77 \times 10^{-2}$
	$2.10 \times 10^{-1}$	2.50	$8.84 \times 10^{-2}$
	$2.20 \times 10^{-1}$	2.47	$8.89 \times 10^{-2}$
<b>Optimal stroke</b> Fig.15 (bottom)	<b><math>2.23 \times 10^{-1}</math></b>	<b>2.56</b>	<b><math>8.90 \times 10^{-2}</math></b>
Abnormal	$2.30 \times 10^{-1}$	2.59	$8.90 \times 10^{-2}$
	$2.50 \times 10^{-1}$	2.85	$8.76 \times 10^{-2}$
	$2.60 \times 10^{-1}$	3.04	$8.54 \times 10^{-2}$
	$2.742 \times 10^{-1}$	4.93	$5.56 \times 10^{-2}$
Limaçon	$2.500 \times 10^{-1}$	3.35	$7.46 \times 10^{-2}$

**Table 3** Geometric efficiency for the abnormal stroke and different normal strokes with the mechanical cost.

#### 4.5 Algorithm to compute the centers of swimming

Next, we present as an application of the previously developed normal form the construction of the center of swimming. To simplify the computations, we shall restrict to the Euclidean case.

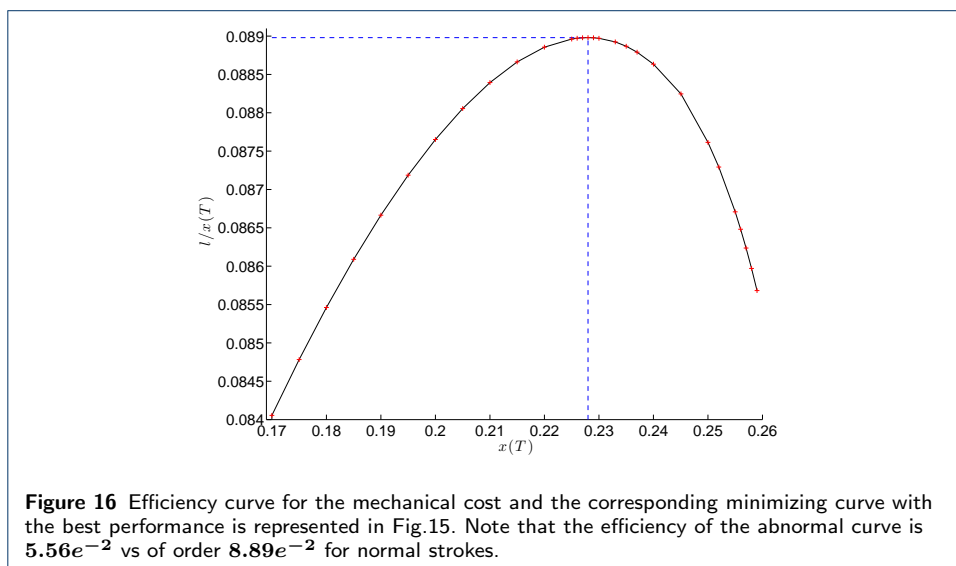
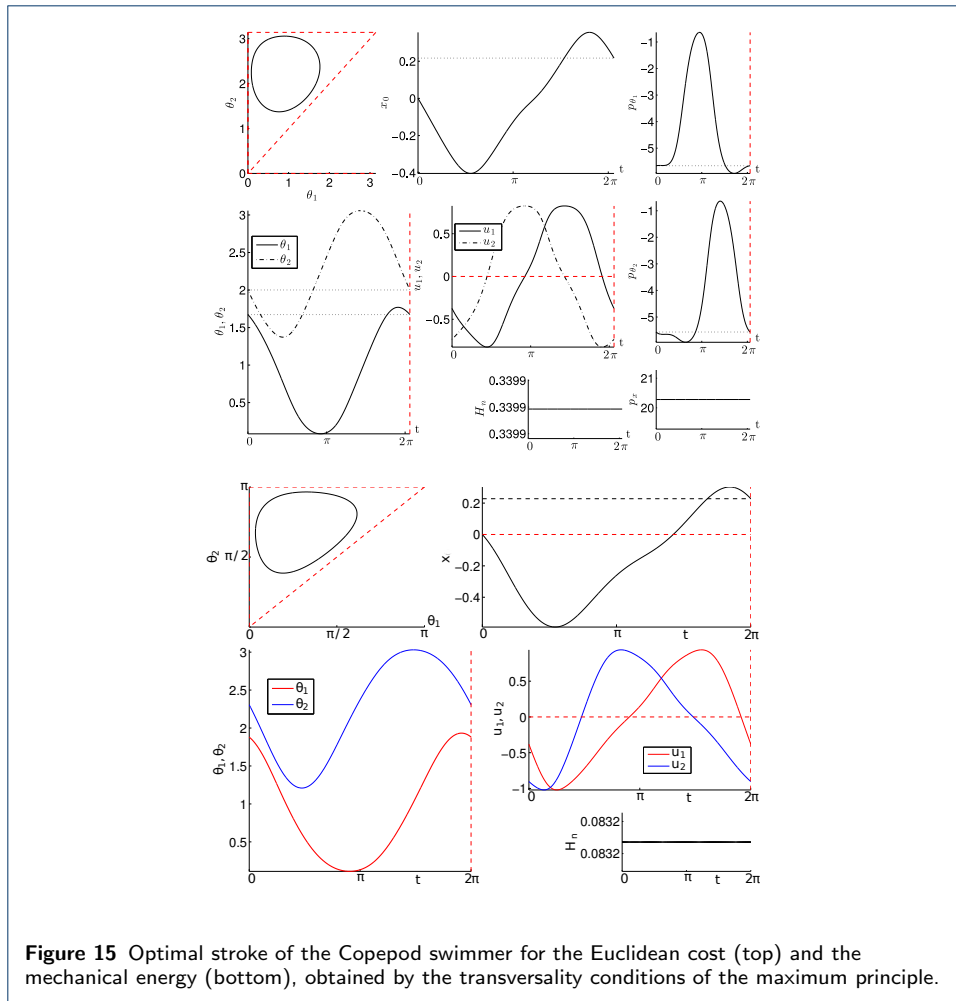
**Lemma 2** *The calculation of the privileged coordinates  $(x, y, z)$  near  $(\theta_1(0), \theta_2(0), 0) \in \text{Interior}(\mathcal{T} \times \mathbb{R})$  with respective weight  $(1, 1, 2)$  provides the link between the physical coordinates and the coordinates of the normal form. In particular, the displacement variable  $x_0$  cannot be identified to the  $z$ -variable since for the Heisenberg-Brockett-Dido model we have that  $\dot{z} > 0$  and hence  $z$  is always increasing, contrary to the copepod swimmer where one stroke produces always forward and backward displacement.*

*Proof* We first introduce the translation:

$$x = \theta_1 - \theta_1(0), \quad y = \theta_2 - \theta_2(0),$$

and then use a transformation of the form:

$$z = x_0 - c_1 x - c_2 y \quad (c_1, c_2 \text{ constants})$$



coupling  $x_0$  and  $\theta$  as a first step to construct the privileged coordinates. □

*Geometric remark.* Further transformations lead to identify the model of order  $-1$  to the model of order zero as a consequence of Theorem 3. Hence, up to this identification, it leads to deform the one-parameter family of symmetric geodesic circles of the Heisenberg-Brockett-Dido case into a one parameter family of simple closed curves in the  $(x_0, \theta)$ -space, see Fig.18. The transformation  $\varphi$  couples in general  $\theta$  with the displacement variables.

To guarantee that the geometric analysis preserves the distinction between shape and displacement variables, we must restrict the calculations to the subgroup  $\mathcal{G}'$  where local diffeomorphisms  $\varphi$  are preserving the  $\theta$ -space.

A tedious but straightforward computation leads to the following result.

**Proposition 10** *Let  $\theta(0) = (\theta_1(0), \pi - \theta_1(0))$  be on the symmetry axis  $\Sigma : \theta_2 = \pi - \theta_1$ . Then the only points where the reduction to the normal form of order 0 is not coupling  $\theta$  and  $x_0$  are described by:*

$$\cos^4 \theta_1(0) + 3 \cos^2 \theta_1(0) - 2 = 0$$

and corresponds to  $\theta_1(0) \simeq 0.723688$ .

Moreover  $(\theta_1(0), \pi - \theta_1(0))$  corresponds to the center of swimming of Fig.13, (top, Euclidean case).

**Remark 2** *This gives another algorithm to compute the center vs the extrema of the swimming curvature. But note that strokes are not with constant curvature.*

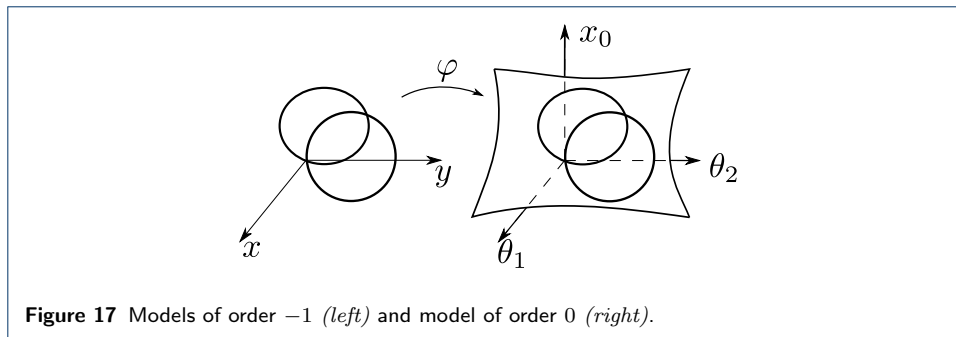
**Proposition 11** *At the center the normal form of order 0 (for the  $\mathcal{G}'$  action) is*

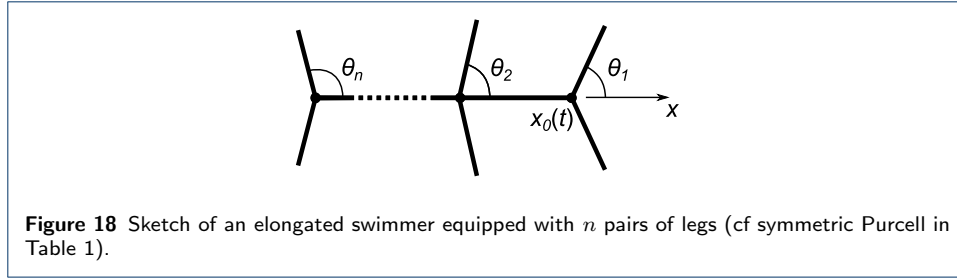
$$F_1(x, y, z) = \frac{\partial}{\partial x} + \frac{y}{2} (1 + Q(x, y)) \frac{\partial}{\partial z},$$

$$F_2(x, y, z) = \frac{\partial}{\partial y} - \frac{x}{2} (1 + Q(x, y)) \frac{\partial}{\partial z}$$

where

$$Q(x, y) = -0.7165898586 x^2 - 0.7379854942 y^2.$$





## 5 3-links copepod, theory and experimental observations

### 5.1 Physical Model

In Section 2 we introduced several models of micro-swimmers. In [20] the model was generalized to allow asymmetry, leading to a wider class of swimmers that can translate and rotate freely and corresponding to generalization of the original Purcell swimmer. However, in these earlier models the governing equations can change when adjacent legs come together and form a bundle of legs. For mathematical convenience we avoid any possibility of bundling by considering the pairs of legs to be sufficiently far apart as formulated below. In this model we represent each leg by a slender rigid rod of unit length and small diameter  $\varepsilon$ , and the elongated body by another rigid rod of length  $2\ell$  and diameter  $2\ell\varepsilon$ , see Fig.18. The axis of the body is parametrized by  $(x_0 - s)\mathbf{e}_x$ , where  $x_0$  is the position of the ‘head’ of the swimmer in the unit direction  $\mathbf{e}_x = (1, 0)$  along the  $x$  axis of the elongated body, and  $s$  is a parameter in the range  $0 \leq s \leq 2\ell$ . The axis along the  $i$ th leg is parametrized by  $s$  in the range  $0 \leq s \leq 1$  according to:

$$\mathbf{x}_i(s, t) = (x_0(t) - x_i)\mathbf{e}_x + s\mathbf{n}_i(t), \quad (18)$$

where  $x_i$  is the distance from the head to the pivot point of the  $i$ th pair of legs, and  $\mathbf{n}_i = (\cos \theta_i, \sin \theta_i)$  is the unit direction along the axis of the  $i$ th leg, which makes an angle  $\theta_i$  with the  $x$  axis. By taking the derivative with respect to time  $t$  we obtain the velocity  $\dot{\mathbf{x}}$ , which is related to the local force density  $\mathbf{f}(s, t)$  according to the leading-order slender-body approximation for Stokes flow

$$\dot{\mathbf{x}} = \frac{\ln(2/\varepsilon)}{4\pi\eta}(\mathbf{I} + \mathbf{nn}) \cdot \mathbf{f}, \quad (19)$$

where  $\eta$  is the viscosity of the surrounding fluid and  $\mathbf{n}$  is the unit tangent, which is either  $\mathbf{e}_x$  along the elongated body or  $\mathbf{n}_i$  along the  $i$ th leg. By rearranging this relation and imposing the constraint that the total force on the swimmer is negligible at low Reynolds number, we obtain the governing equation of motion

$$\dot{x}_0 = \frac{\sum_{i=1}^n \dot{\theta}_i \sin \theta_i}{\ell + \sum_{i=1}^n (1 + \sin^2 \theta_i)}. \quad (20)$$

Note that the governing equation is independent of  $\eta$  and the spacing between adjacent pairs of legs. We hypothesize that the appendages are positioned on the body of the micro-swimmer such that they can intersect when looking at a 2-dimensional



top view while in reality they are not colliding. This feature seems to be especially important when abrupt changes in orientations are needed to for instance escape a predator. However, we are here analyzing translational displacements only and observations suggest that in this case the micro-swimmers appendages are restricted to strokes satisfying

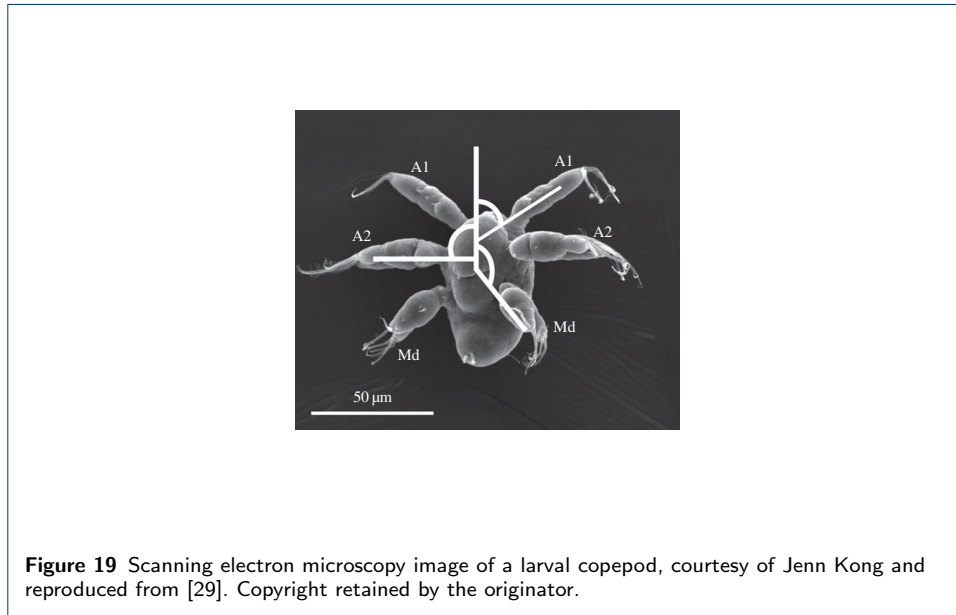
$$\{\theta; \theta_1 \leq \theta_2 \leq \theta_3, \theta_i \in [0, \pi]\}. \quad (21)$$

### 5.2 3-Links

In this section we focus on larval copepods with three pairs of legs, see Fig.19 for an image of a nauplius. They have an unsegmented body, three pairs of appendages (antennules, antennae, and mandibles), and also possess a single naupliar eye. The equations of motion are:

$$\begin{aligned} \dot{q}(t) &= \sum_{i=1}^3 u_i(t) F_i(q(t)), \\ F_i &= \frac{\sin \theta_i}{\Delta} \frac{\partial}{\partial x_0} + \frac{\partial}{\partial \theta_i}, \quad i = 1, 2, 3 \end{aligned}$$

where  $\Delta(\theta) = l + 3 + \sin^2 \theta_1 + \sin^2 \theta_2 + \sin^2 \theta_3$ . From observations, the nauplius



displays physical constraints on the positioning of his legs. More precisely, the two front appendages (A1) on Figure 22 show a variation  $\in [5^\circ, 130^\circ]$ . The second pair of appendages constraint is that  $\theta_2 \in [40^\circ, 135^\circ]$  (A2), and  $\theta_3 \in [110^\circ, 160^\circ]$  (Md). Associated with the constraints (21), we obtain that the angle variables must belong to a trapezoidal prisme and are described by a set of the form:

$$\mathcal{T}_{prism} = \{\theta \in [0, 2\pi]^3; \theta_i \in [\theta_i^{\min}, \theta_i^{\max}], \theta_1 \leq \theta_2 \leq \theta_3\}$$

This set is the extension of the triangle  $\mathcal{T}$  we had when dealing with the 2-link micro-swimmer. Since it is unclear on whether these are real physical constraints

or a deliberate choice from the nauplius we will assume in the future that  $\theta_i^{\min} = 0$  and  $\theta_i^{\max} = 180$  for all  $i$  (i.e. we have a simplex).

Below we analyze the abnormal geodesics and correlate our results with observations on the locomotion of the nauplius made in a laboratory setting.

### 5.2.1 Abnormal geodesics

Differentiating the maximization conditions from the maximum principle:  $H_i(q, p) = \langle p, F_i(q) \rangle = 0$  for  $i = 1, 2, 3$  we obtain:

$$O(q(t), p(t))u(t) = 0$$

where  $O$  is a  $3 \times 3$  skew-symmetric matrix whose entries are given by  $O_{ij} = \langle p, [F_i, F_j](q) \rangle := H_{ij}(q, p)$ . The rank of the matrix  $O$  determines the existence of abnormal controls. Since the rank must be even, an odd skew-symmetric matrix is always singular. We here explicit the case  $\text{rank } O = 0$ , the situation corresponding to  $\text{rank } O = 2$  is described in [20] and it is shown that the solutions do not produce any displacement. First note that:

$$[F_i, F_j](q) = \frac{2 \sin \theta_i \sin \theta_j (\cos \theta_j - \cos \theta_i)}{\Delta} \frac{\partial}{\partial x_0}$$

which implies that  $[F_i, F_j]$  is everywhere linearly independent from the span generated by the vector fields  $\{F_1, F_2, F_3\}$  provided it is not zero.

**Rank  $O = 0$ .** From the maximum principle we have that  $p \neq 0$  and the remark above stating that  $[F_i, F_j](q) \notin \text{span}\{F_1(q), F_2(q), F_3(q)\}$  if  $[F_i, F_j](q) \neq 0$ , we can deduce that  $[F_i, F_j](q) = 0$  holds along an abnormal curve for  $i, j = 1, 2, 3$ . This is equivalent to:

$$\sin \theta_i \sin \theta_j (\cos \theta_j - \cos \theta_i) = 0$$

for all  $i, j \in \{1, 2, 3\}$ . As described in [20] there are four cases to study and we obtain the following result.

**Proposition 12** *Abnormal arcs belong to the vertex and edges of the simplex:*

$$\{\theta; \theta_1 \leq \theta_2 \leq \theta_3, \theta_i \in [0, \pi]\},$$

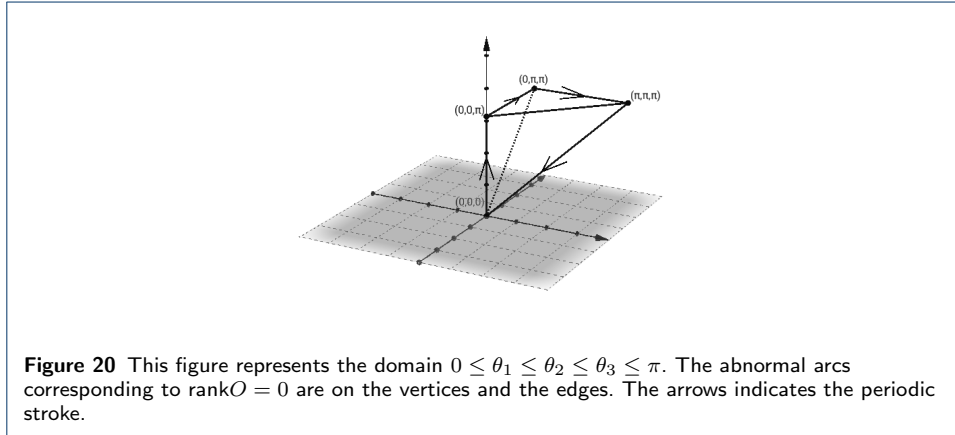
and when parametrized by arc-length on  $[0, \pi]$  correspond to:

- Two legs are fixed and one is moving

$$t \rightarrow \begin{cases} (0, 0, t) \\ (0, t, \pi) \\ (t\pi, \pi) \end{cases}$$

- One leg is fixed and two are moving simultaneously  $t \rightarrow \begin{cases} (0, t, t) \\ (t, t, \pi) \end{cases}$
- Three legs are moving simultaneously  $t \rightarrow (t, t, t)$

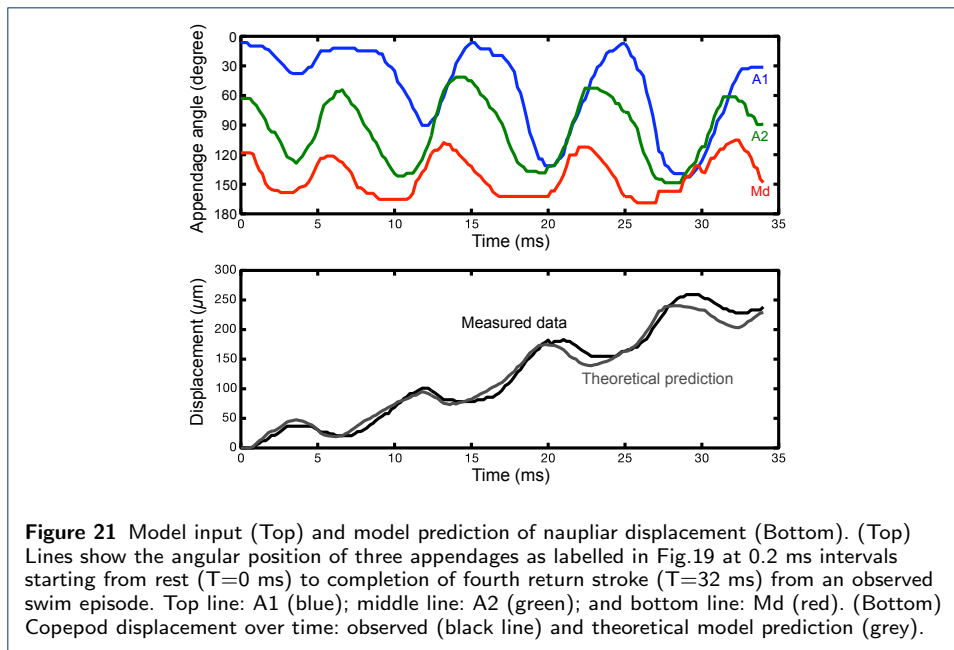
On Fig. 20 we display the prism of constraints which is formed by the interior and boundary of the domain. An abnormal stroke is a periodic motion formed by a concatenation of motions along the edges of the domain. It corresponds to a sequential paddling as introduced in [41] for the elongated body. In that same paper it is observed that sinusoidal and sequential paddling generate comparable displacements but efficiency is higher with sinusoidal paddling.



### 5.2.2 Experimental observations

Experimental observations were conducted on a larval copepod (stage 5 nauplius) by the authors of [29]. On Figure 16 experimental data and model output for a four-cycle swim episode can be seen with the angular measurements used as model input for the theoretical prediction (gray line) shown in bottom picture. It can be observed that angular excursions for this nauplius increased over the first three cycles, especially for antenna A1 for which it nearly quadrupled. As explained in [29], there is strong agreement between the experimental data and the predicted displacement, particularly for the first 20 ms, validating the basic approximations of the model. It can be seen on the bottom picture that the displacement per cycle is increasing which is a result of the increases in amplitude of antenna A1, this suggest that the amplitude of a single appendage excursion can impact the displacement of the nauplius.

Figure 22 displays over a 1.5 cycles of swim sequence the appendage angles of what is referred to in [29] the power (from 15 to about 21 seconds) and return strokes (from 21 to about 24 seconds). As noted before, the appendages on the back (Md) display a physical constraint restricting their amplitude to  $[110^\circ, 160^\circ]$ , respectively  $\theta_2 \in [40^\circ, 135^\circ]$  for (A2) and  $\in [5^\circ, 130^\circ]$  for (A1). However, observations on predator escape show the ability for the nauplius to extremely rapidly change its orientation and overcome the limitations on the angular variables stated here. It can be observed that the back appendages starts the power stroke to move toward  $180^\circ$  at first while the other two pairs of legs position themselves to maximize the amplitude they will use. Once they reach their constraint (first for the second pair of legs) they start moving toward the back of the nauplius. The phase shift created during this power stroke between the three pairs of appendages maximizes displacement forward. The return stroke objective is to minimize backward displacement



to obtain the best net displacement, this is done by coordinating the three pair of legs together.

On Figure 23 we compare the abnormal and observed periodic sequential strokes. The observed one is a close approximation taken from measurement found in Figure 22. It is clearly observed that while the abnormal curve is a concatenation of the edges of the triangular prism of constraints, the observed period strokes belongs to the inside and reflect the, possibly self-imposed, constraints on the appendage angles. However, both strokes are based on the idea of sequential paddling, the main difference resides in the fact that the real copepod takes advantage at the beginning of the strokes to repositioned two of his appendages to eventually maximize their amplitudes (acting like a break as well).

### 5.3 Robotics copepod

In this section we present some preliminary results on a robotics copepod. The main challenge is to mimic the low Reynolds number conditions, and therefore the characteristics of the nauplius environment, while rescaling it to a macroscopic scale. Toward this goal, the experiments presented here are conducted in silicone oil, which is a liquid polymerized siloxane with organic side chains. The robotics copepod is designed for one-dimensional displacement only and displays two pairs of legs. The main objective is to build a mechanical device and set-up that demonstrates the need for decoupled swimming strategies to produce horizontal displacement.

The main features that we tried to keep with the robotic device is the low Reynolds number assumption (met by using a special oil), as well as the one regarding the slim legs to minimize fluid interaction between them. The primary difficulty is to prevent the electronic to get in contact with the oil as it would get damaged permanently. For this reason, and after several trials and iterations, the model has been designed to accommodate a horizontal rail crossing through the body to guarantee its stability on the water.

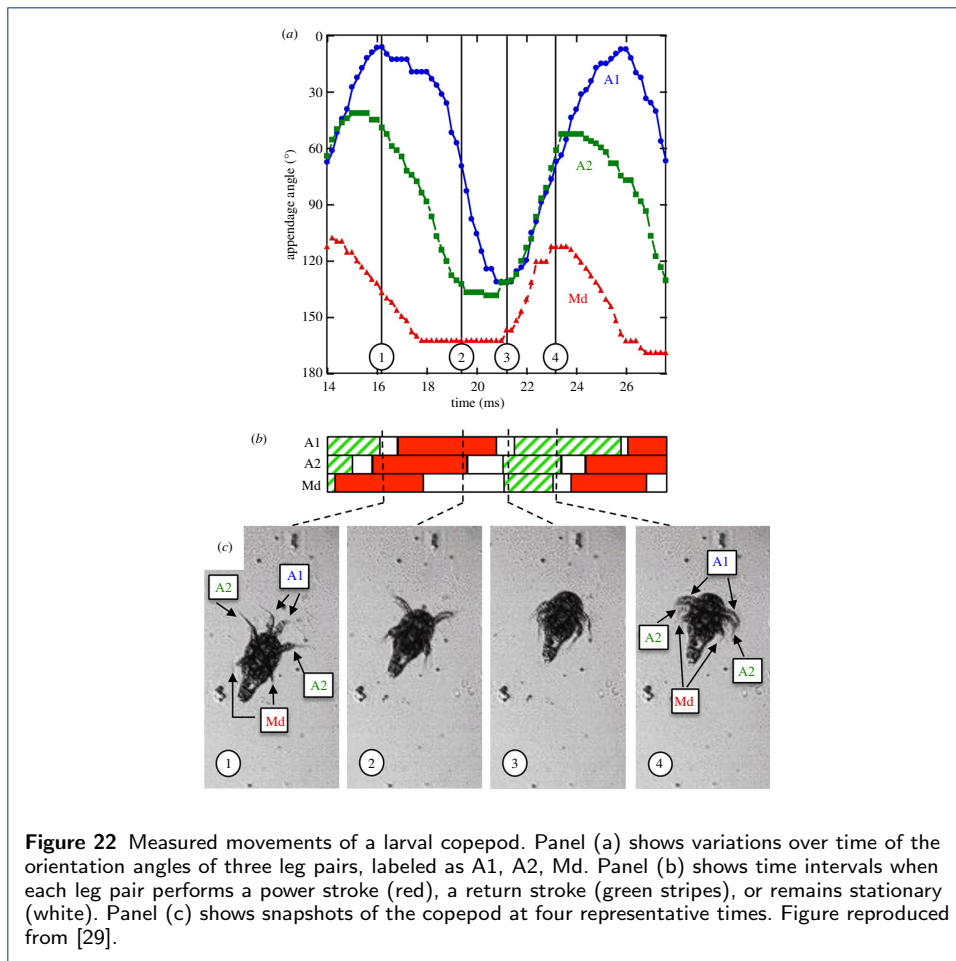


**Figure 22** Measured movements of a larval copepod. Panel (a) shows variations over time of the orientation angles of three leg pairs, labeled as A1, A2, Md. Panel (b) shows time intervals when each leg pair performs a power stroke (red), a return stroke (green stripes), or remains stationary (white). Panel (c) shows snapshots of the copepod at four representative times. Figure reproduced from [29].

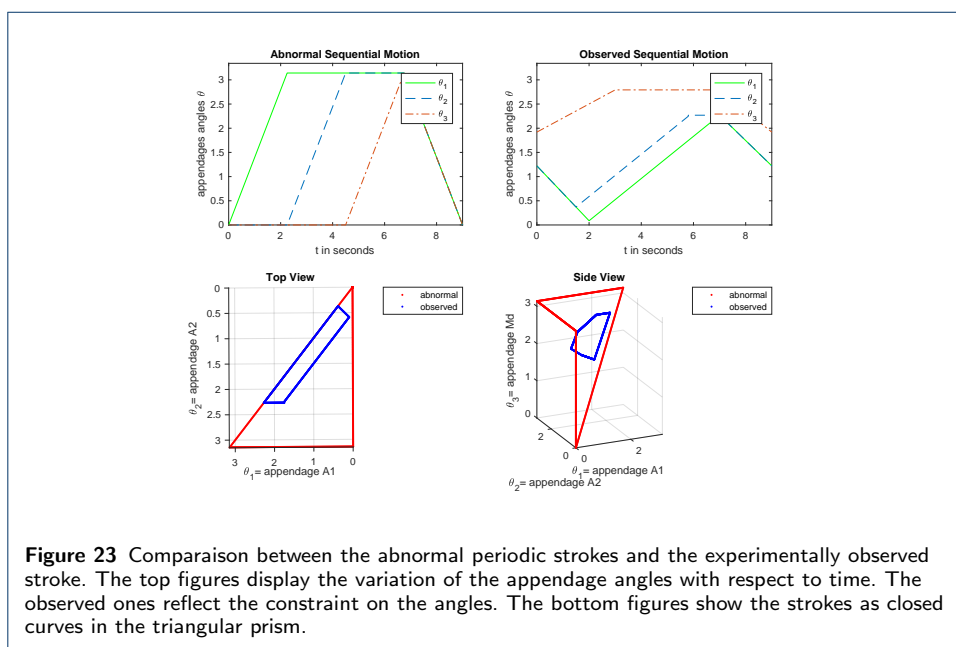
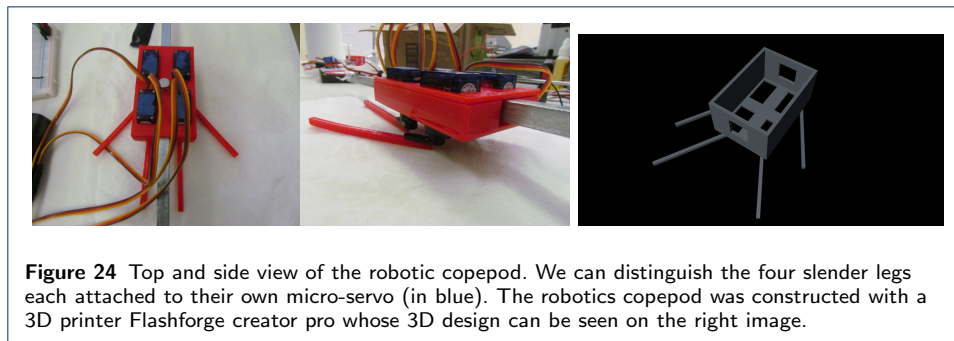


**Figure 23** Comparison between the abnormal periodic strokes and the experimentally observed stroke. The top figures display the variation of the appendage angles with respect to time. The observed ones reflect the constraint on the angles. The bottom figures show the strokes as closed curves in the triangular prism.

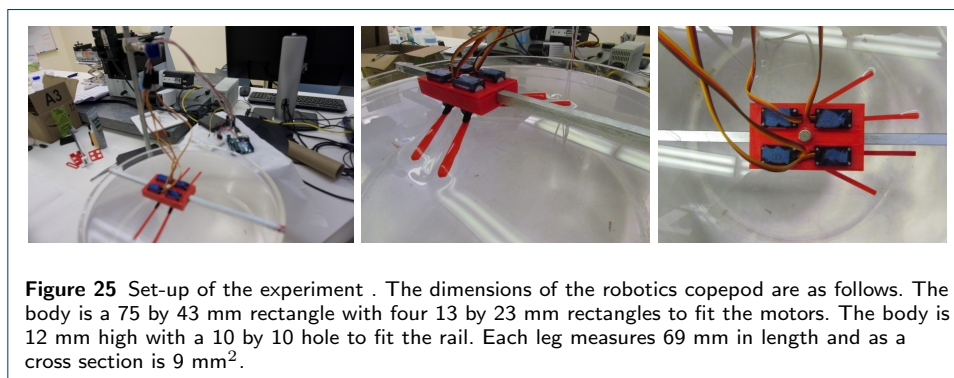
The complete device with the four micro-servos can be seen in Figure 24. It is connected to an Arduino board that is kept outside the testing basin, and the cable from the motors to the Arduino do not touch the oil which prevent additional drag to interfere with the motion.



### 5.3.1 Experiments

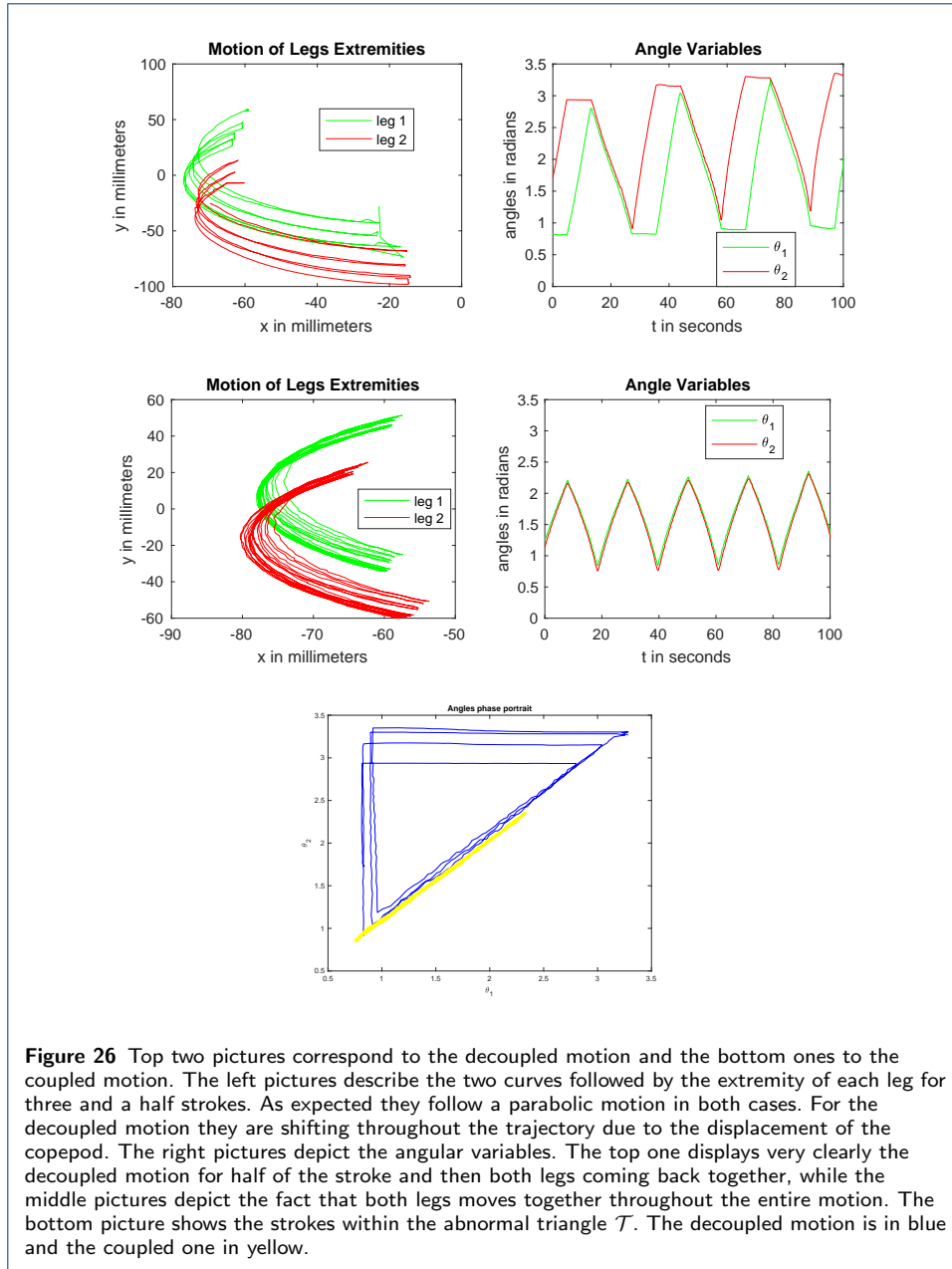
As mentioned above, the experiment we present here is designed to illustrate the necessity of decoupling motion of the links to produce one-dimensional displacement. Figure 25 shows the set-up for the experiment, the copepod seats on the silicon oil in a circular tank of 304.8 mm diameter and with its legs right underneath the surface of the water. The kinematic viscosity of the silicon oil is  $12500 \text{ mm}^2/\text{s}$  at room temperature. Since the length of a leg is 69 mm and the maximum angular velocity for the legs over our experiments is 0.16 radians/s, we obtain  $Re = \frac{69^2 * 0.16}{12500} = 0.06$ .

Two motions will be analyzed, one decoupled sequential motion and one coupled. Figure 26 displays the angular variables for the sequential decoupled motion that were actually produced by the robotics copepod. These data have been obtained by post-processing the movie to track the extremities of the legs and calculating the angle variables from this. They compare extremely well to the observed sequential motion of the copepod in Figure 23 (but with two legs instead of three).



The displacement can be found in Figure 27. It clearly shows that for the decoupled motion there is displacement, the curve for the horizontal displacement is drifting with each stroke. For the coupled displacement, almost no horizontal motion is observed.

Finally, Figure 28 displays a sequence of snapshots of the decoupled motion for the robotics copepod.



## 6 Conclusion

The aim of this short survey article is to present the combination of mathematical and numeric tools recently introduced in (geometric) optimal control and applicable to analyze the problem of swimming at Low Reynolds number, using the slender body theory for Stokes flow. From this point of view, the simplest model of microswimmers is the so-called "copepod model" which can be observed as the copepod nauplii, an abundant variety of zooplankton and realized as a two-link swimmer-robot. The observation of the biological species allows to validate the adequation between the displacement predicted by the model with the measured displacement. Sub-Riemannian geometry is introduced in the analysis by assuming that microswimmers motion are performed minimizing the expanded mechanical energy. This

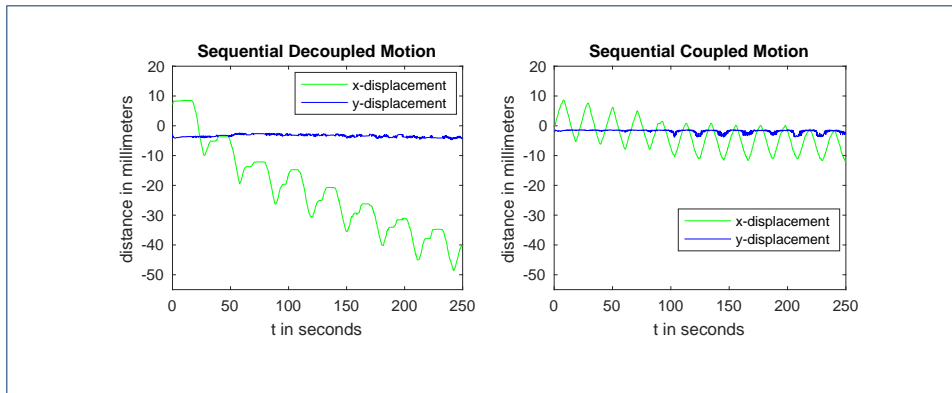


**Figure 27** These graphs compares the displacement produced by the decoupled sequential strokes (left picture) with the displacement from the coupled one (right picture). The motion takes over 5 minutes, the decoupled motion is composed of about 9 strokes while the coupled one does about 13 strokes (a 2/3 ratio which is expected since for the decoupled motion there are three leg motion and two for the coupled one). The drift for the decoupled motion is damped toward the end which is due to the copepod moving closer the boundary of the tank and experiencing its effects. We can observed a slight drift for the coupled motion as well due to our robotics copepod set-up being only an approximation of a Low-Reynolds number environment.

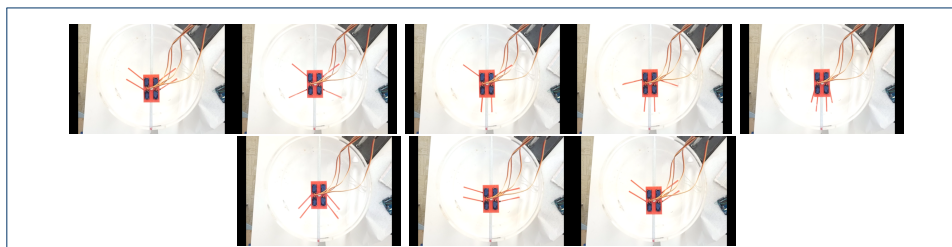


**Figure 28** A sequence of configurations for the copepod during a stroke. The power strokes can be seen in the first 5 snapshots and the return part of the stroke with both legs moving together is displayed in the last three snapshots.

allows for one species to compare the efficiency of different strokes or to compare the efficiency for different species, using the developments of computational methods of SR-geometry. In particular we use estimates of geodesics based on graded normal form, to show the existence of a one parameter family of simple strokes and in this family, only one stroke with a given amplitude is shown to be most efficient. This can be compared to similar result in the literature using a direct approach based on curvature control analysis and Fourier expansion to compute strokes, both approaches are shown to be complementary. The mathematical analysis is neat, abnormal and normal geodesics strokes being related to observed strokes corresponding to "sinusoidal" and sequential paddlings. A further step is to validate the mathematical results using a copepod robot built at the macroscopic scale, to validate the model and the robot observations. Preliminary experimented results are presented based on the abnormal (triangle) stroke and paved the road to further experiments dealing with the most efficient stroke.

The SR-geometry associated to the copepod is related to the well studied 3D-models (Contact, Martinet). Further studies are necessary to analyze the behaviours near the triangle vertices. This is the basis to understand more complicated models, e.g. the Cartan case related to the Purcell swimmer. In this framework this leads to



embed the Contact-Martinet model in the Cartan case, that is to a more intricate micro-local analysis. Also in the frame of optimal control, models taking in account inertia or experimental dissipation can be investigated.

## 7 Declarations

### List of Abbreviations

None.

### Availability of Data and Materials

Data will be made available at the University of Hawaii ScholarSpace  
<https://scholarspace.manoa.hawaii.edu/>

### Funding

DD is partially supported by NSF grant: CBET-1603929. MC is partially supported by the Simons Foundation, award # 359510. BB is partially supported by the ANR Project - DFG Explosys (Grant No. ANR-14-CE35-0013-01;GL203/9-1). JR is supported by the European Research Council (ERC) through an ERC-Advanced Grant for the TAMING project.

### Authors' contributions

All authors contributed to the writing of the paper. BB and JR major contribution is the theoretical and numerical analysis of the results. MC and DD major contribution is the 3-links analysis, experimental observations and robotics device. All authors read and approved the final manuscript.

### Competing interests

The authors declare that they have no competing interests.

### Acknowledgements

We would like to thank Rintaro Hayashi and Amandin Chyba Rabeendran for the pictures and data regarding the robotics copepod.

### Author details

<sup>1</sup>Institut de Mathématiques de Bourgogne, 9, rue Alain Savary, 21078, Dijon, FR. <sup>2</sup>Inria Sophia Antipolis, 2004, Route des Lucioles, 06902, Valbonne, FR. <sup>3</sup>EPF-Ecoles d'Ingénieur(e)s Troyes, 2, rue F. Sastre, 10430, Rosières-près-Troyes, FR. <sup>4</sup>University of Hawaii, 2565 McCarthy the Mall Department of Mathematics University of Hawaii, 96822, Honolulu, HI, USA.

### References

1. A. Agrachev, B. Bonnard, M. Chyba, I. Kupka, Sub-Riemannian sphere in Martinet flat case, *ESAIM Control Optim. Calc. Var.* **2**, 3 (1997) 377–448
2. A. Agrachev, J.P. Gauthier On the Dido problem and plane isoperimetric problems, *Acta Appl. Math.* **57**, 3 (1999) 287–338
3. E. Allgower and K. Georg, Introduction to numerical continuation methods, *Classics in Applied Mathematics, Soc. for Industrial and Applied Math.* **45** Philadelphia, PA, USA, (2003)
4. F. Alouges, A. DeSimone, A. Lefebvre, Optimal strokes for low Reynolds number swimmers: an example, *J. Nonlinear Sci.* **18**, (2008) 277–302
5. J.E. Avron and O. Raz, A geometric theory of swimming: Purcell's swimmer and its symmetrized cousin, *New Journal of Physics* **10**, 6 (2008): 063016
6. G.K. Batchelor, Brownian diffusion of particles with hydrodynamic interactions, *J. Fluid Mech.* **74**, (1976) 1–29
7. A. Bellaïche, The tangent space in sub-Riemannian geometry, *J. Math. Sci. (New York)* **83**, 4 (1997) 461–476

8. P. Bettiol, B. Bonnard, J. Rouot, Optimal strokes at low Reynolds number: a geometric and numerical study of Copepod and Purcell swimmers, to appear *SICON* (2018)
9. P. Bettiol, B. Bonnard, A. Nolot and J. Rouot, Sub-Riemannian geometry and swimming at low Reynolds number: the Copepod case *ESAIM: COCV*, <http://doi.org/10.1051/cocv/2017071>
10. G.A. Bliss, Lectures on the Calculus of Variations, *Chicago Univ. Press*, Chicago, Ill, (1946) ix–296
11. F. Bonnans, D. Giorgi, S. Maingault, P. Martinon and V. Grélard, Bocop - A collection of examples, *Inria Research Report, Project-Team Commands*, **8053**, (2014)
12. B. Bonnard, Feedback equivalence for nonlinear systems and the time optimal control problem, *SIAM J. Control Optim.*, **19**, 6 (1991) 1300–1321
13. B. Bonnard, J.-B. Caillaud, E. Trélat, Second order optimality conditions in the smooth case and applications in optimal control, *ESAIM Control Optim. Calc. Var.* **13**, (2007) 207–236
14. B. Bonnard, M. Chyba, Singular trajectories and their role in control theory, *Mathématiques & Applications* **40**, Springer-Verlag, Berlin (2003)
15. B. Bonnard and D. Sugny, Optimal control with applications in space and quantum dynamics, *AIMS Series on Applied Mathematics* American Institute of Mathematical Sciences, Springfield, **5**, (2012) xvi+283
16. B. Bonnard, E. Trélat, On the role of abnormal minimizers in sub-Riemannian geometry, *Ann. Fac. Sci. Toulouse Math. (6)* **10**, 3 (2001) 405–491
17. R.W. Brockett, Control theory and singular Riemannian geometry, *New directions in applied mathematics* (Cleveland, Ohio, 1980) Springer, New York-Berlin (2016) 11–27
18. T. Chambrier, L. Giraldo and A. Munnier, Optimal strokes for driftless swimmers: A general geometric approach, To appear in *ESAIM Control Optim. Calc. Var.* (2017) <https://doi.org/10.1051/cocv/2017012>
19. El A. Chakir, J.P. Gauthier, I. Kupka, Small sub-Riemannian balls on  $R^3$ , *J. Dynam. Control Systems.* **2**, 3 (1996) 359–421
20. M. Chyba, Y. Kravchenko, O. Markovichenko, D. Takagi, Analysis of efficient strokes for multi-legged microswimmers. *Proceedings of the Conference: 2017 IEEE Conference on Control Technology and Applications (CCTA)*. Kona (2017)
21. S. Childress, Mechanics of swimming and flying. Vol. 2. *Cambridge University Press* (1981).
22. O. Cots, *Contrôle optimal géométrique : méthodes homotopiques et applications*, Phd thesis, Institut Mathématiques de Bourgogne, Dijon, France (2012)
23. R.G. Cox, The motion of long slender bodies in a viscous fluid part 1. general theory, *J. Fluid Mech.*, **44**, 4 (1970) 791–810
24. J. Gray and G. J. Hancock, The propulsion of sea-urchin spermatozoa, *Journal of Experimental Biology*, **32**, (1955) 802–814
25. F. Jean, Control of nonholonomic systems: from sub-Riemannian geometry to motion planning, *Springer Briefs in Mathematics*, Springer, Cham (2014)
26. V. Jurdjevic, Non-Euclidean elastica, *Am. J. Math.*, **117**, (1995) 93–125
27. I. Kupka, Géométrie sous-riemannienne, *Astérisque, Séminaire Bourbaki* **1995/96**, (1997) 351–380
28. D.F. Lawden, Elliptic functions and applications, *Applied Mathematical Sciences*, Springer-Verlag, New York, **80**, (1989)
29. P.H. Lenz, D. Takagi, D.K. Hartline, Choreographed swimming of copepod nauplii, *Journal of The Royal Society Interface* **12**, (2015) 112 20150776
30. M.J. Lighthill, Note on the swimming of slender fish, *J. Fluid Mech.* **9** (1960) 305–317
31. J. Martinet, Singularities of smooth functions and maps. *London Mathematical Society Lecture Note Series*, **58**, Cambridge University Press, Cambridge-New York (1982) xiv+256
32. K. Meyer and G.R. Hall, Introduction to Hamiltonian Dynamical Systems and the N-body Problem, *Applied Math. Sciences*, **94**, Springer-Verlag (1992) 294
33. R. Montgomery, Isoholonomic problems and some applications, *Commun. Math. Phys.* **128**, 3 (1990) 565–592
34. E. Passov, Y. Or, Supplementary notes to: Dynamics of Purcell's three-link microswimmer with a passive elastic tail, *EPJ E* **35** (2012) 1–9
35. H. Poincaré, Sur les lignes géodésiques des surfaces convexes, (French) [On the geodesic lines of convex surfaces] *Trans. Amer. Math. Soc* **6**, 3 (1905) 237–274
36. H. Poincaré, Œuvres. Tome VII, Éditions Jacques Gabay, Sceaux (1996).
37. L.S. Pontryagin, V.G. Boltyanskii, R.V. Gamkrelidze and E.F. Mishchenko, The mathematical theory of optimal processes, *Interscience Publishers John Wiley & Sons, Inc.* New York-London (1962)
38. E.M. Purcell, Life at low Reynolds number, *Am. J. Phys.* **45** (1977) 3–11
39. J. Rouot, Méthodes géométriques et numériques en contrôle optimal et applications au transfert orbital à poussée faible et à la nage à faible nombre de Reynolds., *Ph.D. thesis, Inria Sophia Antipolis Méditerranée*, France (2016)
40. J. Rouot, P. Bettiol, B. Bonnard, A. Nolot. Optimal control theory and the efficiency of the swimming mechanism of the Copepod Zooplankton, *Proc. 20th IFAC World Congress*, Toulouse (2017)
41. D. Takagi, Swimming with stiff legs at low Reynolds number, *Phys. Rev. E* **92**. (2015)
42. D. Tam and A. E. Hosoi, Optimal stroke patterns for Purcell's three-link swimmer, *Phys. Rev. Lett.*, **98**, 6 (2007) 068105
43. R.B. Vinter, Optimal control, *Systems & Control: Foundations & Applications* (2000) xviii–507
44. Q. Wang and J.L. Speyer, Necessary and sufficient conditions for local optimality of a periodic process, *SIAM J. Control Optim.* **28**, 2 (1990) 482–497
45. V.M. Zakalyukin, Lagrangian and Legendrian singularities, *Funct. Anal. Appl.*, **10** (1976) 23–31
46. M. Zhitomirskii, Typical singularities of differential 1-forms and Pfaffian equations, *American Mathematical Society, Providence, RI*. **113**, (1992)
47. J. Zhu, E. Trélat, M. Cerf, Geometric optimal control and applications to aerospace, *Pacific J. Math. for Industry*, **9**, 8 (2017).